

# Photocharging of Semiconductor Materials: Database, Quantitative Data Analysis, and Application in Organic Synthesis

Oleksandr Savateev

Photocharging or photodoping is a process in which electrons are accumulated in a semiconductor upon bandgap excitation followed by quenching of the photogenerated holes by reductants. In semiconductors with excess of electrons, negative charge is compensated by cations, of which the most ubiquitous is  $H^+$ . Photocharging of semiconductors has been studied since 1980s both from a fundamental perspective and application—as source of electrons and protons for reduction of organic compounds in the dark, solar-to-electric energy conversion, and recently also in the design of autonomous microswimmers. In this review, experimental data collected over 40 years of research are summarized and quantified. Maximum specific concentration of electrons stored in 1 g of a semiconductor, maximum average number of electrons stored per semiconductor particle, initial rate of photocharging, and initial rate of discharging are calculated for six classes of semiconductor materials, Ti-, Zn-, Cd-, In-, W-based and graphitic carbon nitrides. Dependence of these parameters on material specific surface area, particle volume, and other properties is analyzed and trends are derived. A public database of photocharged materials is created to facilitate design of high-performing materials with photocharging function, their application as rechargeable reductants in organic synthesis and development of devices.

semiconductors are actively studied in synthesis of fine organic molecules under illumination with artificial light generated by light-emitting diodes (LEDs) or other light sources.<sup>[3–5]</sup> Regardless of the scale and the reaction they mediate, from a very general standpoint, photocatalysts enable flow of electrons from one reagent to another via photoinduced electron transfer (PET) as schematically shown in **Figure 1**.

Assuming that a reaction mixture is composed of an n-type semiconductor that has a potential of the valence band ( $E_{VB}$ , V vs reference electrode (RE)) more positive than the oxidation potential of the electron donor ( $E(D^+/D)$ , V vs RE) and a potential of the conduction band ( $E_{CB}$ , V vs RE) more negative than the reduction potential of the electron acceptor ( $E(A/A^-)$ , V vs RE), the driving force ( $\Delta G^0$ , eV) of the corresponding PET may be expressed by equations<sup>[6,7]</sup>

$$\Delta G_{Ox}^0 = e(E_{CB} - E(A/A^-)) \quad (1)$$

$$\Delta G_{Red}^0 = e(E(D^+/D) - E_{VB}) \quad (2)$$

## 1. Introduction

Taming the energy of visible light by means of semiconductor materials to enable desirable chemical reactions has been a central research topic for many generations of researchers since the middle of the 20th century.<sup>[1]</sup> Today, the scope of applications is enormous. In the context of synthesis of useful molecules rather than degradation of pollutants, semiconductors (SCs) are considered as primary photocatalysts in large-scale full water splitting under outdoor sun light.<sup>[2]</sup> On smaller laboratory scale

where  $e$  is elementary charge. In the context of this review, subscripts “Ox” and “Red” in Equations (1) and (2), respectively, refer to oxidation and reduction of the SC.


Whether it is full water splitting or organic photocatalysis, the energy of a photon is stored in the form of exciton (bound hole–electron pair) or free hole and electron for tens of picoseconds up to hundreds of microseconds.<sup>[8,9]</sup> As dictated by Marcus theory, the rate of electron transfer ( $k_{ET}$ ) depends on the driving force ( $\Delta G_{Red}^0$  and  $\Delta G_{Ox}^0$ )<sup>[10]</sup>

$$k_{ET} = A \exp\left(-\frac{(\lambda + \Delta G^0)^2}{4\lambda k_B T}\right) \quad (3)$$

where  $A$  is the proportional coefficient that depends on the electronic coupling between partners engaged in electron transfer reaction, which in the context of this review are a photoexcited SC particle and either electron acceptor or electron donor;  $\Delta G^0$  is the driving force of the reaction as defined by Equations (1) and (2);  $\lambda$  is the reorganization term, eV;  $k_B$  is the Boltzman constant, and  $T$  is temperature, K.

As  $k_{ET}$  depends on many parameters (Equation (3)), in general, electron transfer between photoexcited semiconductor particle (SCP) and electron acceptor/electron donor is asymmetric.<sup>[11]</sup> If,

O. Savateev  
Colloid Chemistry Department  
Max Planck Institute of Colloids and Interfaces  
Am Mühlenberg 1  
14476 Potsdam, Germany  
E-mail: oleksandr.savatieiev@mpikg.mpg.de

 The ORCID identification number(s) for the author(s) of this article can be found under <https://doi.org/10.1002/aenm.202200352>.

© 2022 The Authors. Advanced Energy Materials published by Wiley-VCH GmbH. This is an open access article under the terms of the Creative Commons Attribution-NonCommercial License, which permits use, distribution and reproduction in any medium, provided the original work is properly cited and is not used for commercial purposes.

DOI: 10.1002/aenm.202200352

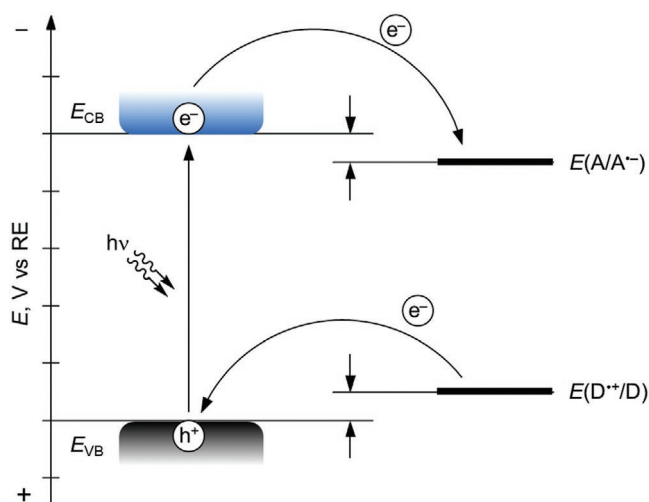


**Figure 1.** Schematic representation of the PET between photoexcited semiconductor, electron donor (ED), and electron acceptor (EA).

for example, an electron donor is oxidized by the photogenerated holes faster than an electron acceptor is reduced by the electrons,<sup>[12,13]</sup> at any juncture there will be slight excess of electrons in the semiconductor particle than holes. Such asymmetry in concentration of charges is maintained under continuous illumination. Once light is off, the remaining electrons are quenched by the omnipresent electron acceptor molecules.

Strong asymmetry in electron transfer emerges when either electron donor or electron acceptor is eliminated from the reaction mixture. It is equivalent to the situation when, for example, oxidation potential of any component of the reaction mixture (any organic or inorganic molecule including solvent) is more positive than the semiconductor VB potential. As inferred from Equation (2), the driving force is absent ( $\Delta G^0_{Red} > 0$ ). Therefore, thermodynamics prohibits such process. Kinetically such process is still possible (Equation (3)), but it is slow to have application in preparative photocatalysis. Similar logic is applicable when any component of the reaction mixture has reduction potential more negative than the semiconductor CB potential. Therefore, the semiconductor may accumulate either holes or electrons, while the lifetime of such stored charges exceeds seconds, days, and even weeks.<sup>[12,14]</sup> In this review, discussion will revolve around semiconductors charged with electrons as much more studied class of materials.

Photochemically reduced SCP, materials that possess excess of electrons, have been known as early as the 1980s.<sup>[15,16]</sup> For example, irradiation of a suspension of  $TiO_2$  particles in the presence of electron donor, such as ethanol, under anaerobic conditions with UV light gives the excited state with the hole–electron pair (Figure 2). Quenching the hole at the expense of ethanol gives a particle with the excess of electrons in the conduction band, while charge-compensating  $H^+$  are either stored in the double layer—a layer formed by the negatively charged surface of metal oxide particle and positive counter ions, or intercalate into the bulk of SCP.<sup>[18–20]</sup> In this review, photocharged SCPs are denoted as  $SCP(e^-/H^+)$ , when the stoichiometry of electron donor interaction with SCP is unknown. When the number of  $e^-/H^+$  transferred between the molecule of electron donor and SCP is known, as in Figure 2, indices

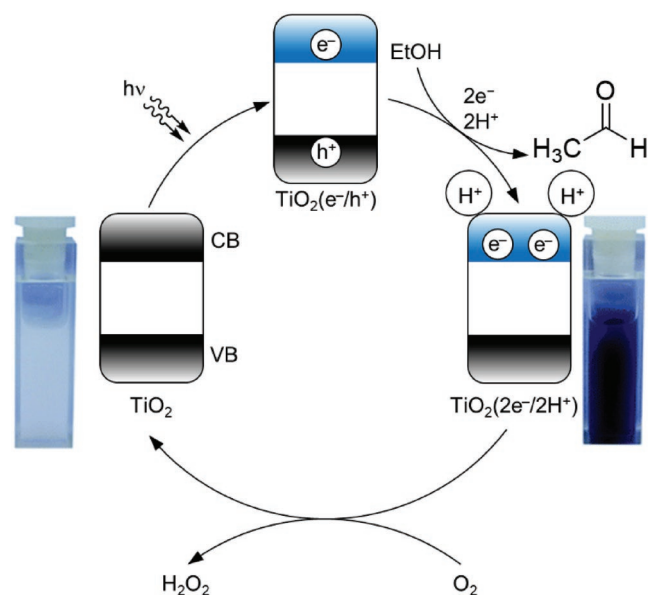


**Figure 2.** Schematic mechanism of model  $TiO_2$  particles photocharging and discharging in dark. Photographs of  $TiO_2$  suspension (white) and  $TiO_2(2e^-/2H^+)$  (darkblue). Reproduced with permission.<sup>[17]</sup> Copyright 2019, Royal Society of Chemistry.

before  $e^-/H^+$  will be used. Capital “H” represents proton and should not be confused with holes that are denoted with lower-case letter “h”. If, for example, lithium cation ( $Li^+$ ) or other charge-compensating cation ( $X^+$ ) is added to the SCP upon photocharging, such SCPs are denoted as  $SCP(e^-/Li^+)$  and  $SCP(e^-/X^+)$ , respectively. More detailed analysis of the photocharged SCP structure change exerted by accumulation of electrons is discussed in Section 2.2.

As will be shown in Sections 6–8, most of materials studied in photocharging are “classical” semiconductors, primarily  $TiO_2$ , ZnO, and CdS. In particular, Bahnemann and co-workers summarized in several reviews trapping of either holes or electrons in  $TiO_2$ , which is the most studied semiconductor material.<sup>[21–23]</sup> Less numerous are the examples of  $Fe_2O_3$ ,<sup>[24]</sup>  $MnO_2$ ,<sup>[25]</sup>  $CeO_2$ ,<sup>[26,27]</sup> and  $NiO$ <sup>[28]</sup> photoreduction. Photochromic effect in  $WO_3$  semiconductors and tungsten oxoclusters, on the other hand, was studied for several decades.<sup>[29–33]</sup>

However, there is emerging interest in ionic photochargeable graphitic carbon nitride (gCN) materials.<sup>[13,34–36]</sup> Ideal structures of these materials are depicted in Figure 3. All these materials are composed of heptazine units, in which both C and N are  $sp^2$ -hybridized. Heptazine units are interconnected either via  $-NH-$  or deprotonated imide groups and form layers. The layers are assembled into a 3D structure via van der Waals forces. This structural feature is reflected in the general name for carbon nitrides—“graphitic.” More specifically, the structure of cyanamide-functionalized poly(heptazine imide) (NCN-PHI, Figure 3a) is terminated by negatively charged cyanamide-groups, while  $K^+$  located in the pores, serve as counter ions.<sup>[37]</sup> For example, concentration of cyanamide-groups in 100 nm sheet was estimated to be 5–12%, which means that every 8th to 20th heptazine unit is missing and replaced by NCN groups.<sup>[38]</sup> Schlomberg et al. concluded that  $K^+$  ions in the pores are solvated by 7 water molecules. Tarakina et al. determined that in potassium poly(heptazine imide) (K-PHI, Figure 3b)  $K^+$  ions

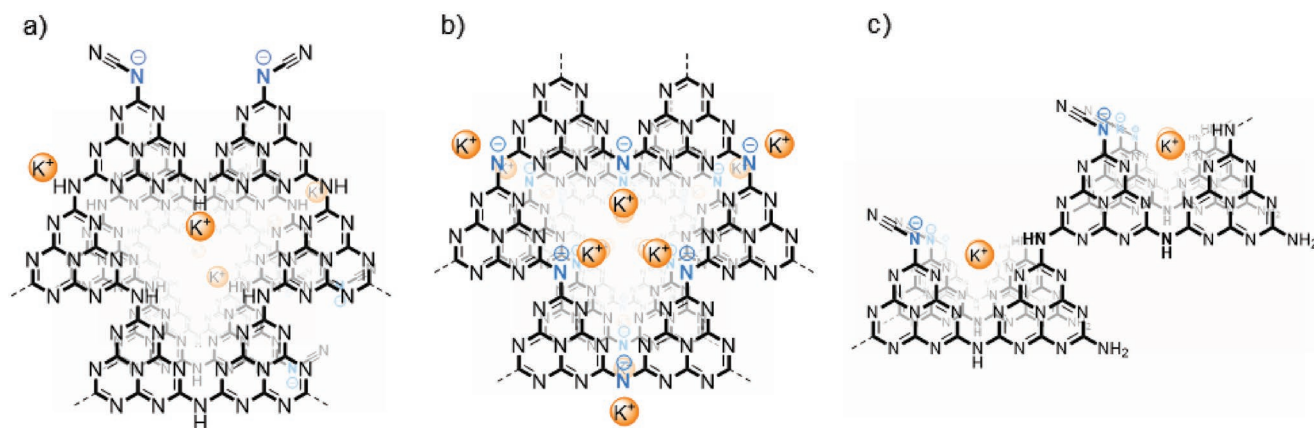


**Figure 3.** Ideal structures of ionic photochargeable graphitic carbon nitride-based materials. a) NCN-PHI. b) K-PHI. c) NCN-CN<sub>x</sub>.

are located closer to the center of the channels and in between layers.<sup>[39]</sup> Sahoo et al. modeled structures of several metal poly(heptazine imide)s and found that in K-PHI and Mg-PHI cations are in the pores between the layers, while in Au-PHI and Ru-PHI cations are in the same plane with PHI layer.<sup>[40]</sup> Using X-ray absorption spectroscopy data, da Silva et al. found that in Fe-PHI, metal cations are in the pores between the layers coordinated by 4 nitrogen atoms—two from each neighboring layer.<sup>[41]</sup> The structure of cyanamide-functionalized heptazine-based polymer (NCN-CN<sub>x</sub>, Figure 3c) is represented by zigzag-like strands of heptazine units.<sup>[13,34]</sup> The strands are arranged into 2D layers via hydrogen bonding (not shown in Figure 3c), similar to melon-type graphitic carbon nitride followed by packing into 3D structured via van der Waals forces.<sup>[42]</sup>

Apart from moderate optical gap,  $\approx 2.7$  eV, microporous polar structure of materials shown in Figure 3 makes them very different compared to nonporous metal oxide nanoparticles and covalent graphitic carbon nitrides.<sup>[43]</sup> Cation containing PHIs demonstrate at least two orders of magnitude higher ion conductivity compared to electron conductivity.<sup>[44]</sup> Due to the diameter of hydrated Na<sup>+</sup> ion ( $\approx 0.72$  nm) that matches perfectly the pore diameter ( $\approx 0.76$  nm) in PHI, this material demonstrates roughly one order of magnitude higher conductivity,  $2.5 \pm 1.0 \times 10^{-6}$  S cm<sup>-1</sup> at 42% relative humidity, compared to K-PHI and Li-PHI.

Ti-based metal organic frameworks (MOFs), such as MIL-125,<sup>[45,46]</sup> NH<sub>2</sub>-MIL-125,<sup>[47]</sup> COK-69,<sup>[48]</sup> and the MOF based on the redox-active Preyssler anion linked with Co(H<sub>2</sub>O)<sub>4</sub><sup>2+</sup> bridging units,<sup>[49]</sup> also undergo photocharging. In addition, there are many examples of hybrid composites based on “classical” metal oxides<sup>[50,51]</sup> including TiO<sub>2</sub> gels.<sup>[52]</sup> Due to similarity in photocharging mechanism, material bandgap excitation followed by hole quenching, and in order to unify notation, all materials analyzed in this review are collectively called semiconductors.

The photocharged SCPs have already been discussed from multiple perspectives. Agrawal et al. summarized localized surface plasmon resonance in degenerately doped semiconductors,<sup>[53]</sup> while Kriegel et al. focused mainly on metal oxides and copper chalcogenides.<sup>[54]</sup> Long and co-workers summarized application of photocharged SCPs as the component of “smart” windows.<sup>[55]</sup> Ghini et al. described possible architectures of devices based on photochargeable materials for harvesting of electromagnetic radiation and energy storage.<sup>[56]</sup> Using

photochargeable PHIs, Sridhar et al. constructed light-driven microswimmers—devices capable for externally controlled autonomous propulsion and delivery of drugs in ionic and biological media.<sup>[57,58]</sup> As accumulation of electrons in SCP is typically accompanied by transfer of ubiquitous protons, photocatalytic reactions under continuous illumination and reactions employing SCP(e<sup>-</sup>/H<sup>+</sup>) in dark proceed via proton-coupled electron transfer (PCET) as summarized by Chen et al.<sup>[59]</sup> Indeed, due to high reactivity of SCP(e<sup>-</sup>/H<sup>+</sup>) they are appealing reagents for reduction of various organic substrates in dark—such reactions were summarized by Kohtani et al.<sup>[60]</sup> Depending on the type of chemical reaction, several terms evolved around such use of photocharged SCPs: “dark” photocatalysis,<sup>[34]</sup> memory catalysis,<sup>[61,62]</sup> around-the-clock photocatalysis,<sup>[63]</sup> and illumination-driven electron accumulation in semiconductors.<sup>[35]</sup>

To design rationally devices and processes employing photochargeable SCPs it is essential to know: 1) how many electrons can a certain SC store, 2) how fast a SC accumulates electrons, and 3) how fast a SC loses electrons upon addition of an oxidant in dark. More precise definition of the first parameter is maximum concentration of electrons in fully charged state, which can be expressed in moles of added electrons per gram of SCPs ( $\delta_{\max}$ , mol g<sup>-1</sup>) or maximum average number of electrons added per SC particle ( $\langle n_{\max} \rangle$ ).<sup>[64]</sup> Alternatively, this parameter is equivalent to maximum doping degree ( $N_{\max}$ , cm<sup>-3</sup>), which is a number of electrons added per 1 cm<sup>3</sup> of a material.<sup>[64]</sup> The second parameter is related to kinetics of SCPs photocharging, which can be quantitatively described as initial rate of SCPs photocharging in moles of added electrons per gram of SCPs per second ( $R_{\text{PC}}$ , mol g<sup>-1</sup> s<sup>-1</sup>). The third parameter describes kinetics of SCPs(e<sup>-</sup>/X<sup>+</sup>) discharging in dark. It can be quantified via initial rate of electron loss by the photocharged SCP upon addition of an electron acceptor, in moles of electrons per gram of SCP per second ( $R_{\text{DC}}$ , mol g<sup>-1</sup> s<sup>-1</sup>).

$\delta_{\max}$ ,  $\langle n_{\max} \rangle$ ,  $R_{\text{PC}}$ ,  $R_{\text{DC}}$  obviously depend on the structure of SCPs: type of the SCP—TiO<sub>2</sub> versus ZnO;<sup>[65]</sup> elemental composition—pure TiO<sub>2</sub> versus TiO<sub>2</sub> doped with elements, such as vanadium;<sup>[66]</sup> crystal structure—anatase versus anatase:rutile mixture versus amorphous TiO<sub>2</sub>;<sup>[67]</sup> diameter—sub-nanometer clusters composed of only 10 Ti atoms versus macrosized particles of TiO<sub>2</sub>;<sup>[68]</sup> morphology—nonporous nanoparticles of TiO<sub>2</sub> versus Ti-based MOF MIL-125,<sup>[45,46]</sup> etc.

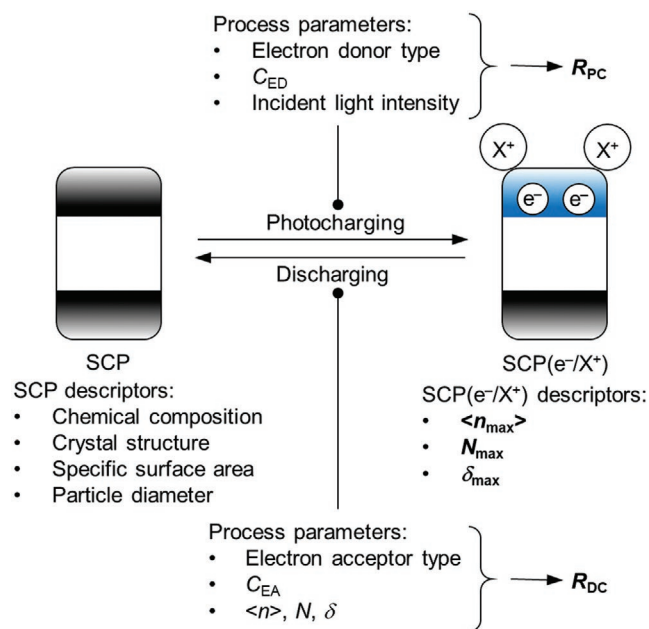


**Figure 4.** Interplay between  $\langle n_{max} \rangle$ ,  $N_{max}$ ,  $\delta_{max}$ , and SCPs properties and process conditions.

In addition,  $\delta_{max}$ ,  $\langle n_{max} \rangle$ , and  $R_{PC}$  may depend on conditions of photocharging, such as: intensity of light; structure of electron donor, and type of counter ion—ethanol, which transfers  $e^-/H^+$ , versus more reductive  $Li[Et_3BH]$ —transfers  $e^-/Li^+$ ;<sup>[64]</sup> concentration of electron donor ( $C_{ED}$ )—few equivalents of remaining ethanol adsorbed at the surface of SCP after solvothermal synthesis versus thousand-fold excess of alcohol in which SCPs are dispersed, etc.

Finally,  $R_{DC}$  may depend on conditions of discharging process, such as: type and therefore reduction potential of an electron acceptor, for example, carbonyl compound, which is reduced to alcohol, versus methylviologen; concentration of an electron acceptor ( $C_{EA}$ ); initial concentration of electrons in a photocharged SCP—photoreduced to a maximum under given conditions degree or photoreduced only partially, etc.

Schematically interplay between properties of the SCPs and conditions of photocharging, and discharging in dark are summarized in **Figure 4**.

More than 40 years of research in the field of materials photocharging gave rich experimental data. Certain dependences have been derived for selected classes of materials, which will be taken as a basis for discussion in Sections 6–8. Nevertheless, in general the data are scattered and not standardized, which impedes deriving fundamental dependences applicable across classes of semiconductor materials.

Related to quantitative  $\langle n_{max} \rangle$  and  $\delta_{max}$  parameters of materials photocharging, this review offers analysis of 52 research articles published in the past 36 years that either explicitly report the abovementioned parameters or provide data sufficient to calculate these parameters (see Section 5). From a set of these references a sample of 303 entries was obtained (**Figure 5a**). The largest number of data points is available for Ti-based materials followed by that based on Zn and gCN (**Figure 5b**). While ZnO nanoparticles are typically described as

crystalline Wurtzite structure, Ti-based materials can be categorized into several groups. These are hybrid  $TiO_2$ -based composites, commercial and certified samples with phase composition ranging from pure anatase to anatase:rutile and pure rutile,<sup>[67]</sup> polyoxotitanate clusters,<sup>[68]</sup> and Ti-based MOFs,<sup>[48]</sup> such as MIL-125 (**Figure 5c**).<sup>[45,46]</sup> In 61% of entries, alcohols, such as EtOH, MeOH, <sup>i</sup>PrOH, were used as electron donors, followed by boranes, such as  $Li[Et_3BH]$  and water, while carbanions are represented by *tert*-butyl lithium and MeMgBr (**Figure 5d**). Counter ion is explicitly specified in 54% of entries, and in 70% of these entries it is  $H^+$ , followed by  $Li^+$  and  $K^+$  (**Figure 5e**).

The objective of the review is to find general dependencies between the parameters of SCPs photocharging ( $R_{PC}$ ), electron storage ( $\langle n_{max} \rangle$ ,  $N_{max}$ ,  $\delta_{max}$ ), discharging ( $R_{DC}$ ), and structure of SCPs (particle volume, specific surface area, etc.) as well as conditions under which SCPs are photocharged and discharged ( $C_{ED}$  and structure of electron donor in photocharging process,  $C_{EA}$  in discharging process, etc.). The database of photocharged materials is created and available at [pccmat.mpikg.mpg.de](http://pccmat.mpikg.mpg.de). Analysis of data is performed and trends are derived. The results intend to facilitate rational development of materials capable to undergo photocharging for energy-storage applications, such as solar batteries, as well as using them as recyclable reductants—source of separated electron–proton pairs in organic synthesis in dark. The latter aspect is elaborated and a summary of chemical reactions mediated by the photocharged SCPs is provided in Section 9. Charging of semiconductors under non-equilibrium conditions, electrochemical, chemical as well as self-doping, is beyond the scope of this review and was summarized earlier.<sup>[69–71]</sup>

## 2. Structure of Photocharged SCPs

This section summarized aspects of SCPs photocharging, which are the most important for data analysis in Sections 6–9—the nature of trapped electrons—either localized at specific atoms or delocalized in the CB; changes in the SCP structure exerted by accumulation of electrons; shift of the Fermi level, and potentials of CB and VB; pathway of electron donors oxidation.

### 2.1. Trapped or Free Electrons?

Typically photocharged  $TiO_2$  colloids exhibit broad absorption band at 400–800 nm, which is likely due to metal-to-metal intervalence transitions (**Table 1**). The extinction coefficient in photocharged  $TiO_2$  colloids is higher than that in isolated  $Ti^{3+}$  complexes (**Table 1**),<sup>[72]</sup> in which simple d–d transitions are responsible for the absorption of light in visible range. In photocharged  $Ti_4$ -oxo-alkoxide clusters, for example, absorption band is broad, while extinction coefficient is  $>150 \text{ M}^{-1} \text{ cm}^{-1}$ ,<sup>[73]</sup> which is similar to  $TiO_2$  colloids rather than isolated  $Ti^{3+}$  complexes.<sup>[74]</sup> Many references conclude that in photocharged  $TiO_2$  colloids added electrons reside on small clusters of Ti-atoms rather than being delocalized in the conduction band over the entire  $TiO_2$  nanoparticle.<sup>[52,75–77]</sup>

In other words, upon  $TiO_2$  photocharging a fraction of  $Ti^{4+}$ -atoms comprising a cluster is reduced to  $Ti^{3+}$ -atoms. In

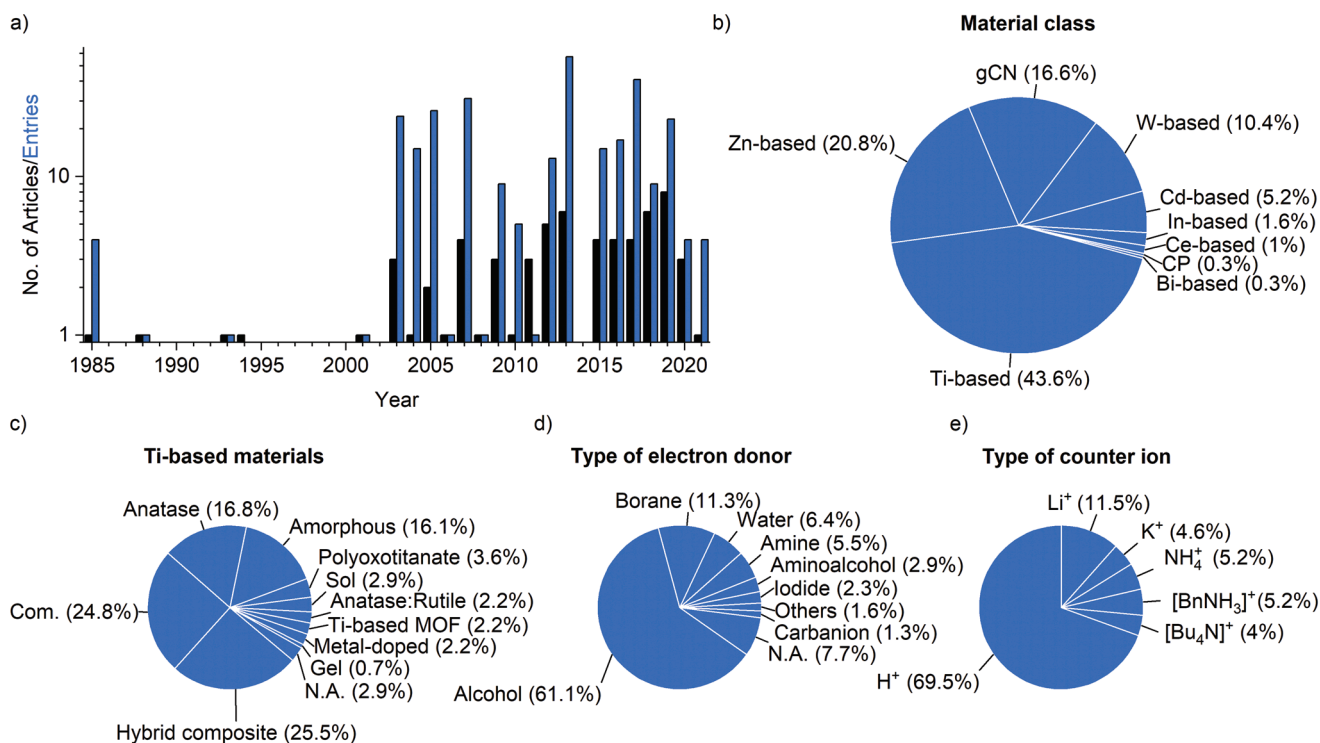


**Figure 5.** Meta-analysis of data used in the review. a) Number of articles (black bars) and the number of entries (blue bars) extracted from the corresponding article published over the years. b) Type of a semiconductor studied in the photocharging. CP – conjugated polymer. c) Categorization of Ti-based materials. Com. – commercial or certified sample; N.A. – phase or additional information related to TiO<sub>2</sub> is not specified in the source reference. d) Type of electron donors used in SCPs photocharging. N.A. – electron donor is not explicitly defined. e) Type of the explicitly specified counter ion in the photocharged SCPs (e<sup>-</sup>/X<sup>+</sup>).

addition, photocharging of TiO<sub>2</sub> to higher degree results in increasing intensity of the absorption peak, but position of the maximum is not changed, which is in agreement with Beer–Lambert law. It also means that despite concentrations of Ti<sup>+3</sup> species in photocharged TiO<sub>2</sub> particle increases, it does not lead to appearance of some sort of collective behavior—clusters of Ti<sup>+4</sup>/Ti<sup>+3</sup>-species within the TiO<sub>2</sub> nanoparticle remain isolated and do not “sense” each other.

On the other hand, photocharged ZnO nanoparticles demonstrate absorption maximum in nIR (Figure 6).<sup>[64,65]</sup> Magnitude of the peak and, what is more important, position of its maximum depends on concentration of electrons in ZnO nanoparticle. Such behavior indicates that the added electrons are free, delocalized in the conduction band.

**Table 1.** Extinction coefficients ( $\epsilon$ ) of selected photocharged TiO<sub>2</sub> colloids and Ti<sup>+3</sup> molecular complexes.

Compound	Particle $d$ [nm]	$\epsilon$ [M <sup>-1</sup> cm <sup>-1</sup> ]	$\lambda$ [nm]	pH	Reference
TiO <sub>2</sub>	3	600	600	2.3 <sup>a)</sup>	[78]
TiO <sub>2</sub>	10	800	780	10 <sup>a)</sup>	[79]
TiO <sub>2</sub>	1.5	470 ± 50	700	2.5 <sup>a)</sup>	[80]
TiO <sub>2</sub>	12	760	650	<7 <sup>a)</sup>	[81]
[Ti(CH <sub>2</sub> OH) <sub>4</sub> Cl <sub>2</sub> ]Cl	- <sup>b)</sup>	4.3	595	- <sup>c)</sup>	[82]
[Ti(C <sub>2</sub> H <sub>5</sub> OH) <sub>4</sub> Cl <sub>2</sub> ]Cl	- <sup>b)</sup>	4.0	595	- <sup>d)</sup>	[82]

<sup>a)</sup>In aqueous solution; <sup>b)</sup>Molecular complex; <sup>c)</sup>In methanol; <sup>d)</sup>In ethanol.

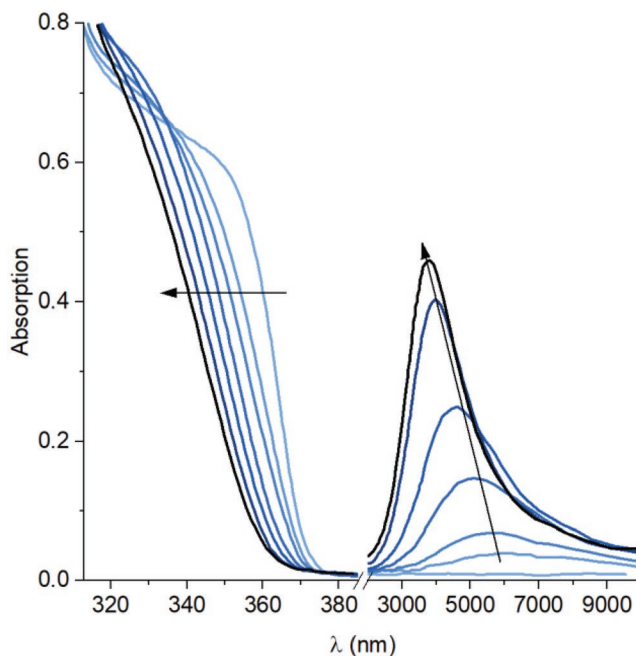


**Figure 6.** Evolution of the absorption peak in nIR upon accumulation of electrons in ZnO. Arrows show blue shift of the absorption peak in IR and bleaching of absorption edge in UV region (explained in Section 4.1) upon illumination. Adapted with permission.<sup>[64]</sup> Copyright 2013, American Chemical Society.

Another piece of evidence that supports delocalized nature of added electrons originates from EPR spectroscopy of photocharged SCPs. Thus, isotropic  $g^*$  values depend on particle diameter.<sup>[83,84]</sup> Accumulation of electrons in the CB increases conductivity of materials.<sup>[49,85]</sup> Regardless of the nature of electrons added to the SCPs, either localized at specific sites or clusters of atoms or delocalized in the CB, both kinds are highly reactive.<sup>[86]</sup> In this review, the state of added electrons is not explicitly differentiated unless it is essential for the discussion.

## 2.2. Explicit and Implicit Counter Ions

In order to maintain electric neutrality, addition of electron(s) must be accompanied by some changes in the structure of the SCP. Transfer of a charge-compensating cation either from the electron donor molecule (see Figure 2) or electrolyte allows to meet this requirement. Such cations are  $H^+$ , alkali ( $Li^+$ ,  $Na^+$ ,  $K^+$ ),<sup>[64]</sup> earth alkaline ( $Mg^{2+}$ ,  $Ca^{2+}$ )<sup>[87]</sup> metal cations, and bulk organic cations, such as decamethylcobaltocenium ( $CoCp^{*2+}$ ), tetrabutylammonium ( $TBA^+$ ),<sup>[87]</sup> and benzylammonium cations.<sup>[35]</sup> Monoatomic cations intercalate into the bulk of the photocharged SCPs,<sup>[87]</sup> while larger cations are stored on the surface. For ZnO in nonaqueous and  $WO_3$  particles in aqueous medium sorption of  $H^+$  is preferential compared to  $Li^+$  cations.<sup>[18,64]</sup> For ZnO nanoparticles, Valdez et al. found that  $N_{max}$  decreases in the order  $Mg^{2+} > Ca^{2+} > H^+$ ,  $Li^+ > Na^+ > TBA^+$ ,  $CoCp^{*2+}$ .<sup>[87]</sup>

In metal oxides, such as  $TiO_2$ , VB is composed of oxygen p-orbitals, while CB—by metal d-orbitals.<sup>[88]</sup> Upon excitation of the SC, which is a kind of photoinduced ligand-to-metal (VB-to-CB) charge transfer, hole is localized at oxygen atom, while electron is at Ti atom (structure  $TiO_2(e^-/h^+)$  in Figure 7a).<sup>[89]</sup> Quenching of the hole by electron donor accompanied by transfer of  $H^+$  produces photocharged  $TiO_2(e^-/H^+)$ .

In Ti-based MOF, quenching of the hole located at oxygen atom followed by trapping a proton from solution or oxidized electron donor (see Section 3 for faith of electron donors) gives a structure with hydroxyl groups.<sup>[45]</sup> Thus, formation of Ti-OD bonds upon photocharging of COK-69, in  $MeOH-d_4$  was confirmed by  $^2H$  MAS NMR as signal at 7.1 ppm.<sup>[48]</sup> Unlike direct excitation of  $TiO_2$ , dye-sensitized photocharging of  $TiO_2$  upon illumination with 520 nm photons gives material with less reactive Ti-H bonds.<sup>[91]</sup>

Unlike Ti that can adopt oxidation states +4 and +3, compounds of  $Zn^{+1}$  are rare and imply formation of Zn-Zn bond as in decamethylzincocene.<sup>[92]</sup> Photocharging of ZnO in excess of  $Li[Et_3BH]$  produces metallic  $Zn^0$ .<sup>[64]</sup> It obviously requires elimination of lattice oxygen and likely to proceed via formation of Zn-Zn bond.

Photodoping of CdSe with organometallic reductants involves dark thermal reduction of surface Cd-Se groups—oxidation state of Se changes from -1 to -2 (Figure 7b), followed by their photooxidation to  $Se^0$  and transfer of an electron to the CB induced by illumination.<sup>[90]</sup>

Accumulation of electrons in SCP unavoidably results in certain structural changes, which can be reversed upon exposure of the photocharged material to oxidants. In this review, if source article explicitly states a type of counter ion added

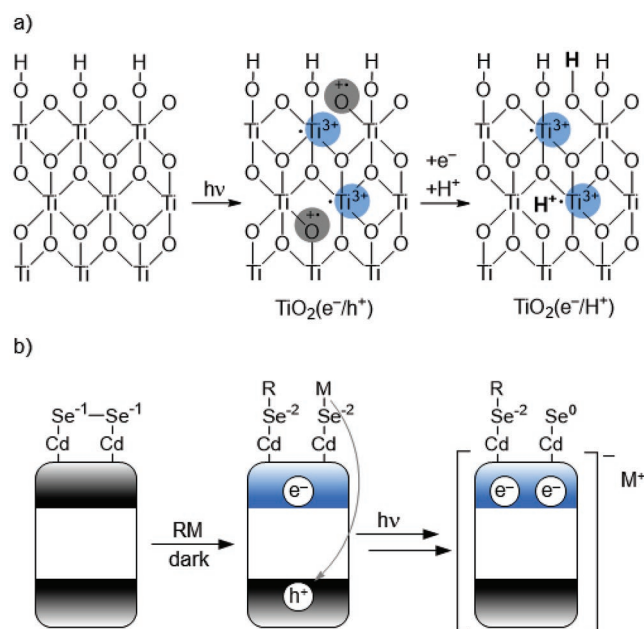


**Figure 7.** Schematic representation of structural changes in semiconductors exerted by accumulation of electrons and charge-compensating ions. a) A fragment of  $TiO_2$  with surface and bulk  $Ti^{3+}$ -sites local structures. b) Changes that occur on the surface of CdSe upon dark prereduction and photocharging. Reproduced with permission.<sup>[90]</sup> Copyright 2016, American Chemical Society.

to photocharged SCP, it is denoted in plain text, for example, SCP( $e^-/H^+$ ). If such information is not provided, the most plausible counter ion is specified in italic, for example, SCP( $e^-/H^+$ ), taking into account composition of the reaction mixture.

## 2.3. The Fermi Level, VB and CB Shifts

Real semiconductor particle contains certain number of defects—imperfection of the crystal structure. These imperfections are, for example, undercoordinated (due to missing oxygen atoms) and hydroxylated Ti-atoms on the surface of  $TiO_2$  (Figure 7a). When considering the band structure, defects may be depicted as energy levels within the bandgap (Figure 8). If the energy level of a defect is close to the VB, it is occupied by electrons. If it is close to the CB then the level remains unoccupied. Ikeda et al. found that in rutile the defects are located 0–0.25 V, while in anatase 0–0.35 eV below the bottom of the conduction band.<sup>[67]</sup> Excitation of electron from the VB to unoccupied energy level induced by a defect requires photons of lower energy. Defects also participate in SCPs photocharging—electrons will first fill the defects close to the CB.

According to the classification proposed by Gamelin et al. photocharged SCPs can be divided into “electronically doped” and “redox-shifted.”<sup>[93]</sup> Figure 8 summarizes such classification and takes into account defective structure of semiconductors.

In electronically doped SCP, potentials of the VB and CB remain the same, while added electrons shift the Fermi level upward (Figure 8a). Such type of doping is implemented, for example, in photocharged CdS nanoparticles.<sup>[94]</sup> In redox shifted

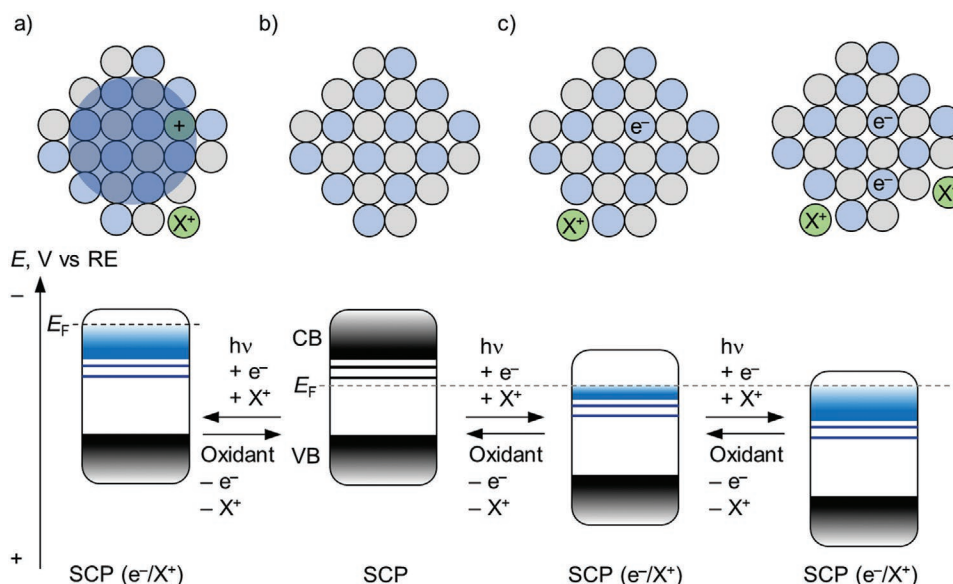


**Figure 8.** Schematic structures of photocharged semiconductors. a) Electronically doped semiconductor. Blue circles represent metal sites. Grey circles represent nonmetallic elements, for example O, S. Green “+” circle represents charge that is embedded into the semiconductor particle and compensated by delocalized electron (large semitransparent circle). b) Original undoped semiconductor. c) Redox-shifted SCPs. Green X<sup>+</sup> circles represent mobile counter ions, such as H<sup>+</sup>, Li<sup>+</sup>, Na<sup>+</sup>, K<sup>+</sup>, etc. (see Section 2.2). Band structure schematic representations are shown below each SCP. Charge-compensating ions on the surface of redox-shifted SCPs are omitted. Adapted with permission.<sup>[20,93]</sup> Copyright 2015 American Chemical Society corresponds to panel a) and b). Copyright 2016 American Chemical Society corresponds to panel c).

SCP, when expressed in electrochemical scale, potentials of both VB and CB are shifted to more positive values. Charge-compensating cations, for example, H<sup>+</sup> in ZnO, exert strong stabilizing effect.<sup>[20]</sup> When photocharging/discharging and the subsequent intercalation/deintercalation of H<sup>+</sup> are completely reversible, shift of the VB and CB potentials shows dynamic behavior levels are shifted upward/downward upon increasing/decreasing concentration of added electrons and H<sup>+</sup>.

Mayer et al. proposed a schematic diagram of the CB that conveniently illustrates ability of different SCPs to attain variable  $N_{\max}$  (Figure 9).<sup>[95]</sup> The structure of the SCP defines the width of the CB and as a result determines  $N_{\max}$ . For example, TiO<sub>2</sub> possess wider CB compared to ZnO, which results in ≈30 times higher  $N_{\max}$ . When photocharged TiO<sub>2</sub>(e<sup>-</sup>/H<sup>+</sup>) and ZnO(e<sup>-</sup>/H<sup>+</sup>) are brought into a contact, electrons flow from one nanoparticle to another until the Fermi levels equilibrate.

From the application standpoint, TiO<sub>2</sub>(e<sup>-</sup>/H<sup>+</sup>) offers higher density of electrons and protons compared to ZnO(e<sup>-</sup>/H<sup>+</sup>). Indeed, there are plenty examples of using photocharged

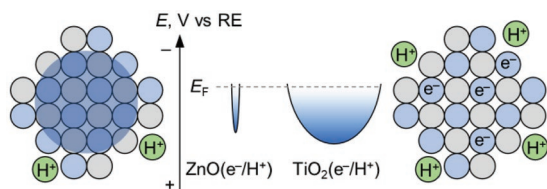


**Figure 9.** Schematic representation of the CB structure of photocharged ZnO(e<sup>-</sup>/H<sup>+</sup>) and TiO<sub>2</sub>(e<sup>-</sup>/H<sup>+</sup>). It is assumed that in ZnO(e<sup>-</sup>/H<sup>+</sup>) added electrons are delocalized in the conduction band, while TiO<sub>2</sub>(e<sup>-</sup>/H<sup>+</sup>) electrons reside at Ti<sup>3+</sup>/Ti<sup>4+</sup> clusters. Reproduced with permission.<sup>[95]</sup> Copyright 2019, American Chemical Society.

TiO<sub>2</sub>(e<sup>-</sup>/H<sup>+</sup>) for reduction of substrates in dark, which are summarized in Section 9, but only few examples of using ZnO(e<sup>-</sup>/H<sup>+</sup>) for this purpose.<sup>[96]</sup>

### 3. Decomposition Pathways of Common Electron Donors

A very general mechanism scheme of alcohols photoinduced oxidation accompanied by SCP charging with e<sup>-</sup>/H<sup>+</sup> is shown in Figure 10a.

For simplicity, it is assumed that SCP is free of any defects—there are no energy levels in the bandgap. VB-to-CB excitation of an SCP gives SCP(e<sup>-</sup>/h<sup>+</sup>) (Step 1). In Step 2, one-electron oxidation of a bound alkoxide molecule followed by transfer of H<sup>+</sup> gives either radical A or radical B and SCP(e<sup>-</sup>/H<sup>+</sup>). Step 2 proceeds likely via PCET, which energetically is more favorable compared to stepwise transfer of an electron and a proton. As a result, it is employed in preparative photocatalysis.<sup>[97–99]</sup> Compared to the radical A, the ketyl radical B is thermodynamically more stable—many compounds of this type, especially benzophenone and fluorenone ketyls, were detected and even isolated.<sup>[100,101]</sup> The ketyl radical B, is characterized by low bond dissociation free energy (BDFE) of ≈26–30 kcal mol<sup>-1</sup> (ref. [102])—hydrogen atom is weakly bond to oxygen. Upon injection of e<sup>-</sup> into the CB of SCP(e<sup>-</sup>/H<sup>+</sup>) accompanied by transfer of H<sup>+</sup>, the radical B is converted into a carbonyl compound and doubles the amount of e<sup>-</sup>/H<sup>+</sup> in SCP. Step 3 proceeds likely via PCET due to the fact that formation of tentative intermediates, protonated ketone [R<sub>2</sub>COH]<sup>+</sup> upon electron transfer, as well as ketone radical anion, [R<sub>2</sub>CO]<sup>-</sup> upon proton transfer, thermodynamically are extremely unfavorable.<sup>[103]</sup>

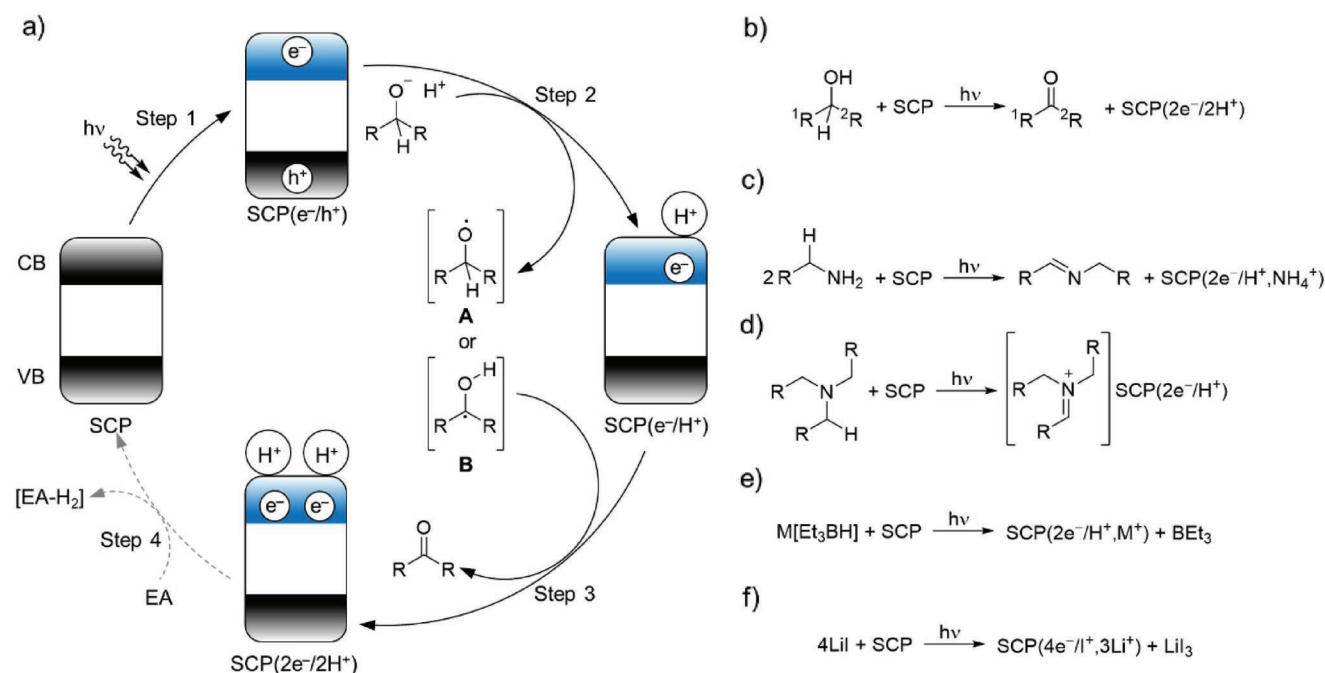


**Figure 10.** Decomposition pathways of different molecules typically used as electron donors in SCPs photocharging. a) A schematic mechanism of alcohols oxidation to aldehyde and SCP photocharging. In order to be consistent with mass balance, the number of  $e^-/H^+$  added to SCP in each step is explicitly specified. b–f) Reaction schemes of alcohols, metal borohydrides, and Lil oxidation accompanied by SCP photocharging.

An experimental piece of evidence for Step 3 was provided by charging of  $TiO_2$  particles dispersion in  $^iPrOH$  upon  $\gamma$ -photolysis.<sup>[80]</sup> In this case,  $\gamma$ -photon cleaves C–H bond and generates  $[Me_2COH]^\cdot$  radical, which in turn injects an electron into the CB of  $TiO_2$ . In this example, however, the mechanism does not involve excitation of electron from VB to CB in  $TiO_2$ . Note that Step 3 does not require energy input—it is downhill due to the fact that the radical **B** is converted into thermodynamically stable  $R_2C(O)$ . Absorption of one photon in Step 1 results in overall transfer of  $2e^-/2H^+$  and therefore called current doubling (Figure 10b).<sup>[104]</sup> Step 4 takes place only if there is a molecule in the reaction mixture capable to accept  $e^-/H^+$  from  $SCP(2e^-/2H^+)$ —EA is converted into hydrogenated form,  $[EA-H_2]$ . Conditions that make this process thermodynamically feasible are discussed in Section 9.

Taking into account available data and general patterns of radicals decomposition, the most important of which is cleavage of  $\beta$ -X–H bond in organic radicals,<sup>[105,106]</sup> Figure 10c–f summarizes products of several electron donors oxidation. Primary amines, such as benzylamine, are decomposed according to the reaction shown in Figure 10c. Peculiar feature of this reaction is that unlike alcohols that transfer  $2e^-/2H^+$  to the SCP, primary amine transfers  $2e^-$ ,  $H^+$ , and  $NH_4^+$ .<sup>[35,107]</sup> Tertiary amines are decomposed according to the pathway shown in Figure 10d. Upon quenching of the photogenerated hole by the nitrogen lone pair and followed by injection of an electron into the CB and a proton from  $\alpha$ -carbon atom iminium cation is formed.<sup>[108]</sup> Metal borohydrides provide  $2e^-/H^+$ ,  $M^+$  upon their oxidation (Figure 10e).<sup>[64]</sup> According to the stoichiometry of iodide anion oxidation to  $I_3^-$ ,  $I^+$  must be formed in equimolar ratio that likely serves as charge-compensating cation upon  $TiO_2$  photocharging (Figure 10f).<sup>[109]</sup> In the context of

net-oxidative photocatalytic reactions, photocharging of SCPs may explain nonzero conversion of substrates in control experiments performed without electron acceptors, such as  $O_2$ .<sup>[110,111]</sup>

## 4. Overview of Methods Used to Determine $\langle n \rangle$ , $N$ , $\delta$ , $R_{PC}$ , and $R_{DC}$

Methods to determine number of added electrons into SCPs have been summarized in several works.<sup>[53,56]</sup> This section provides a summary of techniques that are the most relevant to this review.

### 4.1. Steady-State Absorption Spectroscopy

Considering that photocharged SCPs absorb light in visible range, absorption spectroscopy is a primary technique used to determine  $\langle n \rangle$ ,  $N$ , and  $\delta$ . Note that “max” subscripts are omitted to emphasize that these parameters can be determined for SCPs, which are photocharged only partially. It is especially useful when SCPs form transparent solutions. In this case, knowing extinction of photocharged SCPs and applying Beer–Lambert law, one can obtain concentration of electrons in a sample.<sup>[78]</sup> However, position of absorption maximum and extinction coefficient depend on pH and conditions of photocharging (Table 1). More universal approach consists of measuring the absorption spectra coupled with titration of photocharged SCPs with redox indicators:

- Coordination compounds of  $Fe^{3+}$ —decamethylferrocenium tetrakis[3,5-bis(trifluoromethyl)phenyl]borate  $[FeCp^*_2][BAR_F]$ ,<sup>[112]</sup>  $FeCl_3$  or  $Fe(ClO_4)_3$  followed by complexation of



$\text{Fe}^{2+}$  ions with 1,10-phenanthroline.<sup>[113,114]</sup> One equivalent of  $\text{Fe}^{3+}$  consumes one equivalent of electrons stored in photocharged SCP.

- Methylviologen dichloride ( $\text{MV}^{2+}2\text{Cl}^-$ ). It is reduced to methylviologen radical ( $\text{MV}^+\text{Cl}^-$ ) that has extinction coefficient  $13\,700\text{--}13\,900\text{ M}^{-1}\text{ cm}^{-1}$  at  $606\text{--}609\text{ nm}$  in water, MeOH, EtOH, and acetonitrile.<sup>[115]</sup> Stoichiometry of electron transfer between  $\text{MV}^{2+}2\text{Cl}^-$  and photocharged SCP is 1:1.
- Thionine dyes such as methylene blue that has extinction coefficient  $10^5\text{ M}^{-1}\text{ cm}^{-1}$  at  $655\text{ nm}$  are reduced to *leuco*-form.<sup>[116]</sup> The reduction potentials of thionine dyes are from  $-0.119$  to  $0.064\text{ V}$  versus NHE.<sup>[81]</sup> One equivalent of thionine dye accepts two equivalents of electrons.
- $\text{K}_2\text{Cr}_2\text{O}_7$  is reduced to  $\text{Cr}^{3+}$ .<sup>[117]</sup> One equivalent of  $\text{K}_2\text{Cr}_2\text{O}_7$  removes six equivalents electrons from photocharged SCP.
- 2,4,6-tri(*tert*-butyl)phenoxy radical ( ${}^t\text{Bu}_3\text{ArO}^\bullet$ ) has low extinction coefficient of  $430\text{ M}^{-1}\text{ cm}^{-1}$  at  $620\text{ nm}$ .<sup>[65]</sup>
- 2,2,6,6-tetramethylpiperidine-*N*-oxyl radical (TEMPO) has also low extinction coefficient of  $10.5\text{ M}^{-1}\text{ cm}^{-1}$  at  $475\text{ nm}$ .<sup>[65]</sup>

Absorption signatures of  ${}^t\text{Bu}_3\text{ArO}^\bullet$  and TEMPO are rarely used to quantify number of transferred electrons. Instead amount of phenol and *N*-hydroxylamine formed upon transfer of  $e^-/\text{H}^+$  from  $\text{SCP}(e^-/\text{H}^+)$  is quantified by  ${}^1\text{H}$  NMR spectroscopy.

In case of transparent SCPs solution, the point of titration is determined upon complete quenching of the photocharged SCPs absorption band (Figure 11a) and appearance of the absorption from the oxidant (Figure 11b). Interception of fitting lines gives number of electrons stored in the material (Figure 11c).

Transparent solution of SCPs is also convenient system to track kinetics of photocharging—once intensity of the absorption stops increasing, maximum concentration of electrons is reached.<sup>[118]</sup>

Quantification of number of electrons stored in nontransparent, turbid, colloidal solutions of photocharged SCPs due to light scattering is more challenging. In this case a known mass of a photocharged material is typically treated with the excess of redox indicator followed by absorption spectra measurements.<sup>[35,45]</sup> Knowing the extinction coefficient of the reduced form of the indicator in combination with Beer–Lambert law gives concentration of electrons in the sample.

It must be pointed out that only electrons that possess mobile counter ions can be extracted by the abovementioned oxidants. Electrons whose positive counter ions are embedded into the semiconductor matrix such as  $\text{Al}^{3+}$ -doped  $\text{ZnO}$ <sup>[118]</sup> and  $\text{Sn}^{4+}$ -doped  $\text{In}_2\text{O}_3$ ,<sup>[112]</sup> are chemically inert. Stronger oxidants, such as  $\text{Ce}^{4+}$ ,  $[\text{NO}]^+$ , or  $[\text{N}(4\text{-BrC}_6\text{H}_4)_3]^+$ , can extract some of the electrons, but they also cause irreversible changes in chemical structure of SCPs.<sup>[112]</sup>

When electrons added to the photocharged SCP are free, position of the plasmon peak and its intensity depends on the concentration of electrons—the larger  $N$  the more intense and more blue-shifted is the absorption peak (Figure 6). Applying Drude model to IR spectra of  $\text{SCP}(e^-/\text{X}^+)$ ,<sup>[53]</sup> one can determine concentration of electrons in the photocharged material.<sup>[86,119]</sup>

In addition to the appearance of the absorption band in vis–nIR, photocharging of SCPs bleaches the absorption band

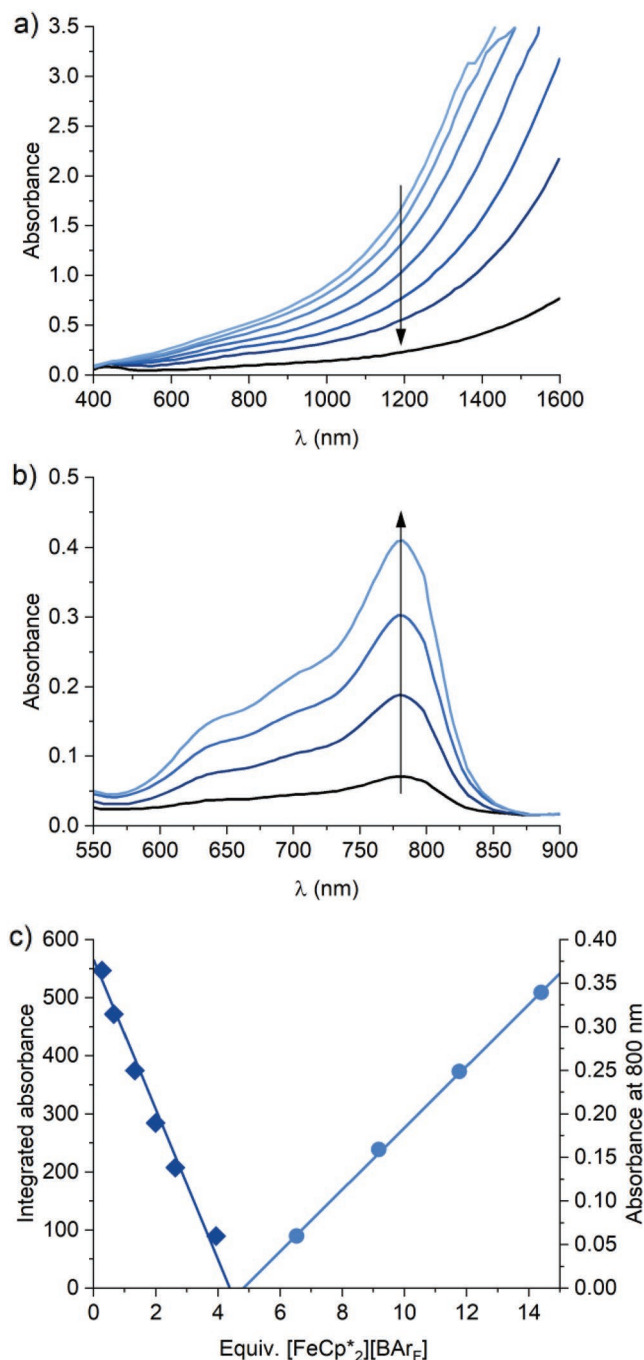


**Figure 11.** Titration of photocharged ZnO nanoparticles with  $[\text{FeCp}^*_2][\text{BARf}]$ . Reproduced with permission.<sup>[64]</sup> Copyright 2013, American Chemical Society.

related to VB-to-CB transitions known as Moss–Burstein shift (Figure 6). Since electronic transitions are only possible between occupied and unoccupied states, filling the bottom of the CB with electrons results in widening of the optical gap—more energetic photons are required to excite electrons from the VB to the unoccupied states in the CB. Intriguing is the fact that photocharged CdSe nanoparticles do not exhibit strong absorption in vis–nIR, while bleaching of the fundamental

absorption band is used to quantify number of electrons added to the nanoparticle.<sup>[69,90,120]</sup> Alternatively, blue-shift of the fundamental absorption band is explained by Stark effect—additional portion of energy is required to compensate inhomogeneous charge distribution caused by polarization of a polaron.<sup>[121]</sup>

#### 4.2. Transient Absorption Spectroscopy

The rate of electron transfer from SCP( $e^-/X^+$ ) to the electron acceptor depends on its driving force (Equation (1))—difference between the CB potential and reduction potential of the oxidant.<sup>[122]</sup> The stopped-flow technique is limited to the processes that occur on the time scale  $>5$  ms or rate constants  $<10^7$   $M^{-1} s^{-1}$  when working with micromolar concentrations of oxidants.<sup>[83]</sup> In case of quenching photocharged SCPs by stronger oxidants, transient absorption spectroscopy appears to be the only suitable technique.<sup>[65]</sup>

#### 4.3. EPR Spectroscopy

Either localized at atoms cluster or delocalized in the CB of semiconductor nanoparticles, added electrons may be observed in the EPR spectra. Howe and Grätzel found that not all electrons that were registered by UV-vis spectroscopy (see Section 4.1) are “visible” in the EPR spectra.<sup>[16]</sup> Thus, at pH 2.2 all electrons stored in 10–15 nm  $TiO_2$  particles are observed by EPR. By adjusting pH to 10, particles grow to 200 nm in diameter and in EPR spectra only 10% of  $Ti^{3+}$  are registered. Such observation may be explained by the relaxation time of paramagnetic  $Ti^{3+}$  sites, which is defined by the metal coordination sphere at pH 10, to be too short. Short relaxation time results in extreme line broadening and as a result absence of a distinct signal in EPR spectrum. For photocharged ZnO, a perfect linear correlation between the  $g$ -values and absorbance at 850 nm was obtained.<sup>[123,124]</sup>

#### 4.4. Electrochemical Methods

A film composed of SCPs that is deposited at the working electrode is remarkably similar to a battery. It can be charged by 1) applying potential, which on the electrochemical scale is more negative than the Fermi level,<sup>[120,125]</sup> and 2) irradiation with light having photon energy greater than optical gap (photocharging). In the first case, injection of electrons is triggered by the electromotive force provided by the potentiostat and charge-compensating cations enter the electrode from the electrolyte.<sup>[126,127]</sup> In the latter case, both electrons and charge-compensating ions are supplied by reductants (see Figure 10). Open-circuit potential (OCP) is equivalent to the Fermi level of electrons in SCPs (Figure 12).

The amount of stored electrons is determined from discharge curves by applying fixed current (Figure 13). Increasing illumination time allows to store greater charge in NCN-PHI as illustrated by longer time required to return electrode potential, the Fermi level, to original values by applying constant discharge current.

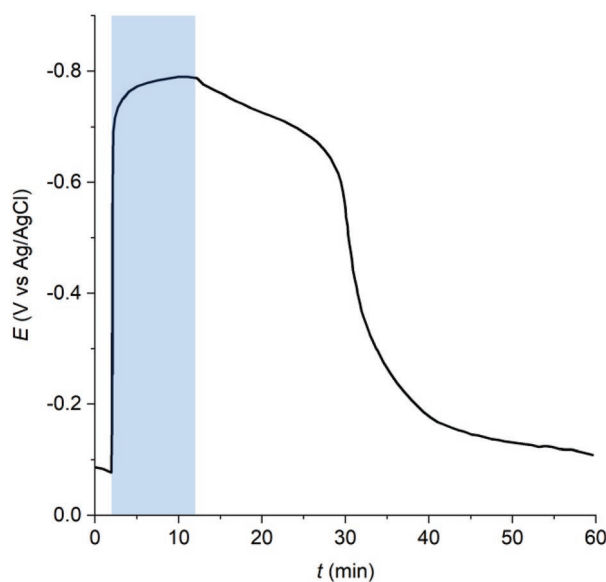


**Figure 12.** OCP of the electrode composed of NCN-PHI particles deposited at FTO. Blue rectangle indicates period of time when the working electrode was illuminated with light. Reproduced with permission.<sup>[37]</sup> Copyright 2018, John Wiley & Sons, Inc.

#### 4.5. Methods that Are Not Based on Absorption Spectra of Photocharged SCPs

When an oxidant, which is capable to accept  $e^-/H^+$  and form a stable product is added in excess versus the amount of electrons stored in photocharged SCP, quantification of the amount of reduced species by standard laboratory techniques, such as NMR in solution, GC-MS, LC-MS, allows determining  $\langle n \rangle$ ,  $N$ , and  $\delta$ . A list of reactions is provided in Section 9.

### 5. Database of Photocharged Materials

In 20% of all entries used for analysis of electron storage in materials (see also Figure 5) in this review, specific surface area ( $S_{SA}$ ) of the studied materials was reported (Figure 14a). In 50% of these cases, it was determined using physical methods, typically  $N_2$  physisorption. In 50% cases commercial material was used and  $S_{SA}$  was taken from the supplier’s material sheet.

Equations (4)–(6) allow to unify data and access both particle diameter ( $d$ ), its volume ( $V_p$ ) and  $S_{SA}$

$$V_p = \frac{4}{3} \pi \left( \frac{d}{2} \right)^3 \quad (4)$$

Surface area ( $S_p$ ,  $nm^2$ ) of a single particle was calculated using Equation (5)

$$S_p = 4\pi \left( \frac{d}{2} \right)^2 \quad (5)$$

$S_{SA}$  of a material ( $m^2 g^{-1}$ ) composed of spherical particles was calculated according to Equation (6)

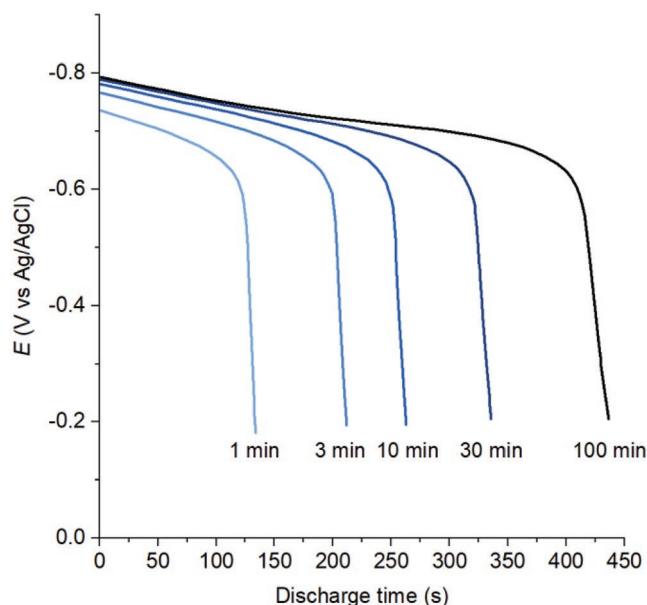


**Figure 13.** Potential of NCN-PHI@FTO working electrode versus time upon setting discharge current at 100 mA g<sup>-1</sup> (normalized per mass unit of NCN-PHI). Time of electrode illumination is shown under each curve. Reproduced with permission.<sup>[37]</sup> Copyright 2018, John Wiley & Sons, Inc.

$$S_{SA} = \frac{S_p \cdot 10^{21}}{V_p \cdot \rho \cdot 10^{18}} \quad (6)$$

where  $\rho$  is gravimetric density of the material, g cm<sup>-3</sup>. It is likely that Equation (6) overestimates real  $S_{SA}$  of materials, since it does not take into account possible sintering of particles. If not available in the reference article, the following gravimetric density of materials was used: ZnO 5.6 g cm<sup>-3</sup>, TiO<sub>2</sub> 3.9 g cm<sup>-3</sup> (amorphous, anatase), K-PHI 1.88 g cm<sup>-3</sup> (X-ray density),<sup>[39]</sup> H-PHI 1.39 g cm<sup>-3</sup> (X-ray density),<sup>[38]</sup> gCN (when crystal structure was not explicitly specified) 2.2 g cm<sup>-3</sup>, In<sub>2</sub>O<sub>3</sub> 6.75 g cm<sup>-3</sup>, CeO<sub>2-x</sub> 7.13 g cm<sup>-3</sup>, CdSe 5.3 g cm<sup>-3</sup>, and WO<sub>3</sub> 7.2 g cm<sup>-3</sup>. Gravimetric density of hybrid composites made of SCPs and metal nanoparticles or two semiconductors was calculated taking into account a fraction and gravimetric density of each component.

Meta-analysis indicates that 25% of all entries explicitly report  $\langle n \rangle$  (Figure 14b),  $N$  is reported in 9% of entries (Figure 14c), and  $\delta$  is reported in 17% of entries (Figure 14d). Using reported data, missing  $\langle n \rangle$ ,  $N$ , and  $\delta$  values were calculated according to Equations (7) and (8)

$$\langle N \rangle = \frac{\langle n \rangle \cdot 10^{21}}{V_p} \quad (7)$$

$$\langle \delta \rangle = \frac{\langle N \rangle}{N_A \cdot \rho} \quad (8)$$

where  $N_A$  is Avogadro number,  $6.02 \times 10^{23}$  mol<sup>-1</sup>.

Still 42% of  $\langle n \rangle$  values, 17% of  $N$  values and 2% of  $\delta$  values are not accessible mainly due to two factors: diameter of nanoparticles was not reported and materials are large particles having complex morphology. Nevertheless, the largest data set

is available for  $\delta$ . Therefore, this parameter will be primarily used in Sections 6–8 to analyze photocharging and discharging of SCPs. Concentration of SCPs ( $C_{SCP}$ , mol[particles] L<sup>-1</sup>) was taken directly from the reference article or calculated according to Equation (9)

$$C_{SCP} = \frac{m_{SCP} \cdot 10^{21}}{\rho \cdot V_p \cdot N_A \cdot V_s} \quad (9)$$

where  $m_{SCP}$  is mass of SCP, g;  $V_s$  is volume of nanoparticles dispersion in a solvent, L.

Data points that were acquired under comparable conditions and accumulate around certain areas in the plots are highlighted with rectangles of specific colors. Data points that follow a trend are highlighted with rhombus. As will be shown in Sections 6–8,  $\langle n \rangle$ ,  $N$ ,  $\delta$ ,  $R_{PC}$ , and  $R_{DC}$  depend on multiple factors, while experimental conditions vary for one source article to another. As a result, data are strongly scattered. Therefore, rectangles and rhombus are more appropriate to highlight trends or absence of trends instead of fitting the data with mathematic functions. Considering that dependences are complex, it is not always possible to reflect all parameters in the plots. Sections 6–8 provide several examples of using the database and support general conclusions related to materials photocharging derived earlier in quantitative fashion. Readers are invited to analyze interactive plots available at TableauPublic<sup>[128]</sup> and pccmat.mpikg.mpg.de for more rigorous analysis.

## 6. Kinetics of SCPs Photocharging

Schematic kinetic curve obtained upon materials photocharging is shown in Figure 15.

Only few articles report a law according to which photocharging of SCPs proceeds.<sup>[18]</sup> Kinetics might change from second order, when concentration of electron donor and SCPs are comparable, to pseudo-first order, when photocharging is performed at large excess of electron donor. In this review initial rate of photocharging ( $R_{PC}$ , mol[electrons] g<sup>-1</sup> s<sup>-1</sup>) is used as the parameter to quantify how fast SCPs accumulate electrons (Figure 15a).  $R_{PC}$  is defined as the first derivative of  $\delta(t)$  at  $t = 0$  according to Equation (10)<sup>[64]</sup>

$$R_{PC} = \left( \frac{d\delta}{dt} \right)_{t=0} = \frac{\Delta\delta}{\Delta t} \quad (10)$$

Due to the limited number of data points typically acquired in the kinetic study and available in reference articles, in this review  $R_{PC}$  is calculated as the ratio between concentration of electrons accumulated in SCPs ( $\Delta\delta$ , the first titration data point) after time  $\Delta t$  of the reaction mixture illumination. It is assumed that at  $t = 0$ , prior illumination of the reaction mixture, concentration of electrons in SCPs is negligibly small. When necessary  $\Delta\delta$  is calculated using data provided in the source article applying Equations (7) and (8). Meta-analysis of data taken for analysis in this section indicates that in 77% of entries saturation was reached—concentration of electrons in the SCP ( $e^-/X^+$ ) reaches plateau (Figure 15b).

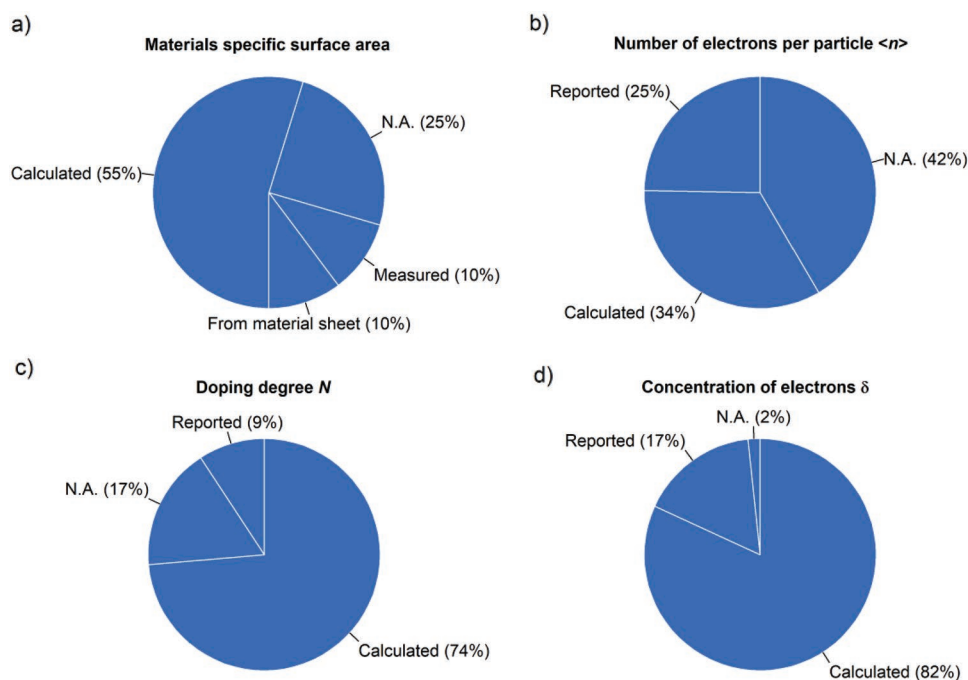


**Figure 14.** Meta-analysis of data used in this review to analyze electron storage in materials. a) Specific surface area of materials. N.A. –  $S_{SA}$  is not reported and characterization of materials is not sufficient to calculate  $S_{SA}$ . b) Number of electrons per particle  $\langle n \rangle$ . c) Doping degree  $N$ . d) Concentration of electrons  $\delta$  in photocharged SCPs.

### 6.1. Dependence of $R_{PC}$ on Concentration of Electron Donor

In Figure 16a,  $R_{PC}$  is plotted versus concentration of electron donor ( $C_{ED}$ ). Photocharging of SCPs has been studied at  $C_{ED}$  ranging from tens of  $\mu\text{M}$ <sup>[90]</sup> up to 25 M (pure methanol).<sup>[18,91,109]</sup> One could expect that SCPs are photocharged faster, when electron donors are used in higher concentration. However,  $R_{PC}$  does not show strong dependence on  $C_{ED}$ . Such result could be rationalized taking into account that in the photocharging experiments, concentration of SCPs is in the range  $10^{-11}$ – $10^{-1}$

mol[particles]  $\text{L}^{-1}$  (Figure 16b), which is still lower compared to  $C_{ED}$ . In order to quantify the excess of electrons per SCP available in the photocharging experiment, parameter  $x_e$  was calculated according to Equation (11)

$$x_e = \frac{k \cdot C_{ED}}{C_{SCP} \cdot \langle n_{max} \rangle} \quad (11)$$

where  $k$  is the number of electrons that is provided by a single electron donor molecule. For primary or secondary alcohols, for example,  $k = 2$  given their oxidation to carbonyl compounds (Figure 10b). Numerator in Equation (11) is equal to the concentration of electrons that are “stored” in electron donor molecules prior illumination, while denominator takes into account concentration of electrons in the photocharged SCPs. Analysis of Figure 16c proves that in the reaction mixture, electrons available for the reaction in the form of reductants are present in at least tenfold excess compared to SCPs.

The structure of electron donor on the other hand strongly affects  $R_{PC}$ . Thus, ZnO particles with the diameter of 5.6 nm are reduced  $\approx 40$  times faster in the presence of borohydrides,  $\text{Li}[\text{Et}_3\text{BH}]$ ,  $\text{K}[\text{Et}_3\text{BH}]$ ,  $\text{Li}[\text{Me}_2\text{NBH}_3]$ ,  $[\text{Bu}_4\text{N}][\text{Et}_3\text{BH}]$ , which are stronger reductants, compared to EtOH.<sup>[64]</sup> However, large excess of borohydrides results in irreversible reduction of ZnO and formation of  $\text{Zn}^0$ . Sorption of  $\text{H}^+$  at ZnO is more preferable compared to  $\text{Li}^+$  as indicated by comparable  $R_{PC}$  values for experiments performed using EtOH and a mixture of EtOH/ $\text{Li}[\text{PF}_6]$ . Despite comparable conditions, different materials are reduced at different rate. In the presence of Li- and Na-borohydrides and even stronger organometallic reductants, such as  $\text{MeMgBr}$ ,  $\text{Me}_2\text{MgBr}$ ,  $^t\text{BuLi}$ , sodium naphthalenide,<sup>[90]</sup> 3.6 nm CdSe particles

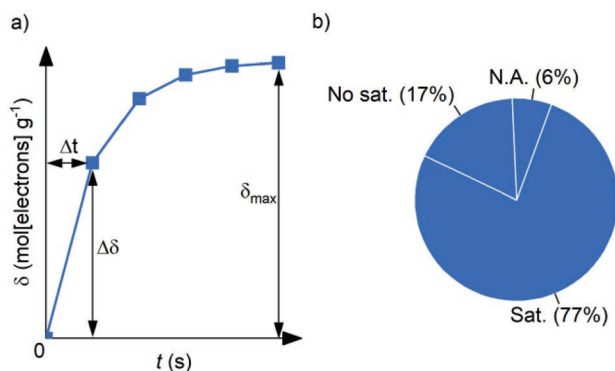


**Figure 15.** Kinetics of photocharging. a) Schematic plot of  $\delta$  versus time of illumination. It is assumed that accumulation of electrons in SCP is described by pseudo-first order equation. b) Meta-analysis of data used in Section 6. Sat. – saturation of SCP with electrons was achieved; No sat. – photocharging was terminated before SCP was saturated with electrons; N.A. – data are not sufficient to conclude whether SCP was saturated with electrons or not.

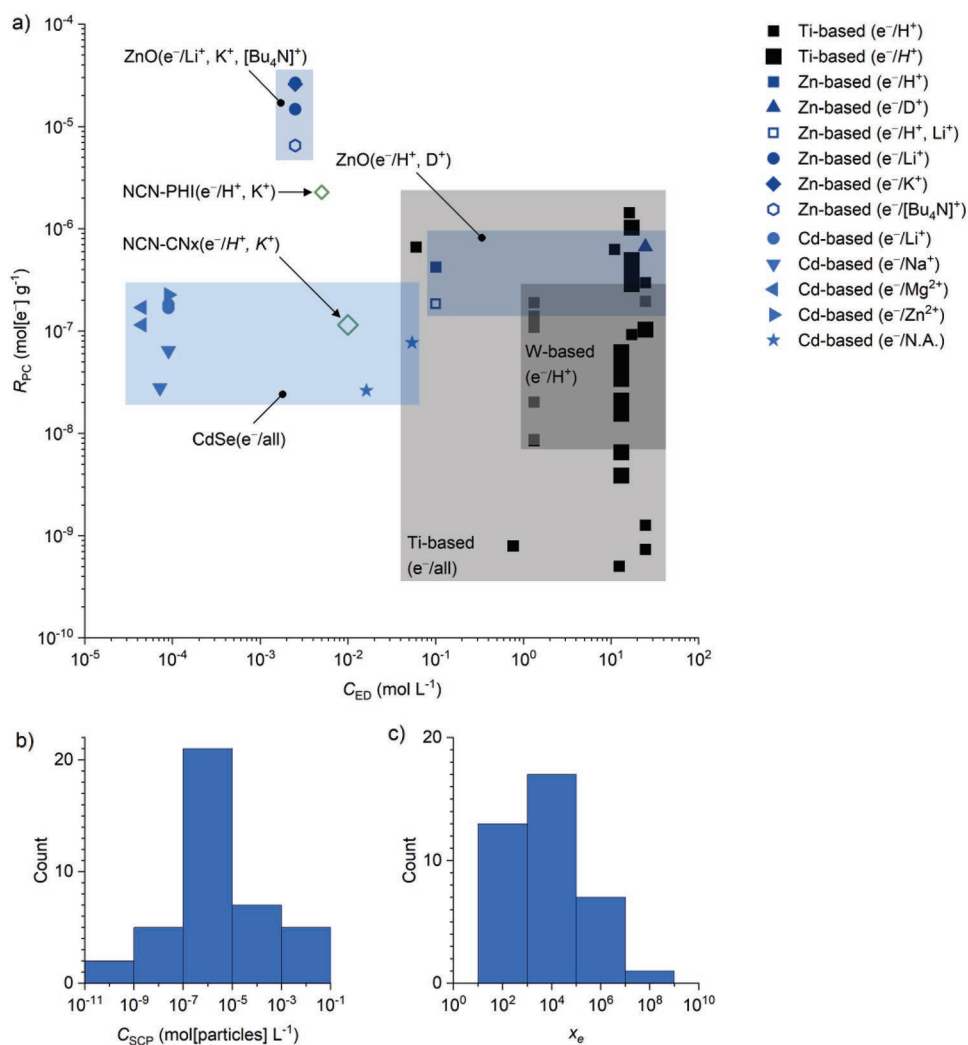


**Figure 16.** Photocharging of SCPs. a) Dependence of  $R_{PC}$  on  $C_{ED}$  plotted in logarithmic scale. b) Distribution of  $C_{SCP}$  values in the photocharging experiments. c) Distribution of  $x_e$  values.

are reduced  $\approx 120$  times slower compared to ZnO nanoparticles.<sup>[64]</sup> NCN-PHI (Figure 3a) is photocharged ten times faster, when the material is deposited as a thin film at FTO,<sup>[37]</sup> compared to a suspension of NCN-CNx in 4-methylbenzyl alcohol.<sup>[34]</sup>

Data for Ti-based materials are strongly scattered by more than three orders of magnitude, which clearly indicates dependence of  $R_{PC}$  on other parameters. Such parameters, for example, are light intensity and presence of additives that could scavenge e<sup>-</sup>/H<sup>+</sup> from photocharged SCPs. Thus,  $R_{PC}$  of 21 nm TiO<sub>2</sub> (anatase:rutile 80:20) suspension in <sup>1</sup>PrOH (13.1 M) is reversibly proportional to concentration of styrene oxide (see also Section 7.1 for the impact of styrene oxide concentration on  $\delta_{max}$ ).<sup>[113]</sup> Photocharging of TiO<sub>2</sub> nanoparticles that includes CB-to-VB excitation under UV light as shown in Figure 2 and 10, proceeds  $\approx 230$  times faster compared to dye sensitized TiO<sub>2</sub> photocharging.<sup>[91]</sup> Hu et al. found that among polyoxotitanates composed of only 12 Ti atoms, those doped with one Zn, Mg or Ca atoms are photocharged up to three times faster compared to undoped polyoxotitanate.<sup>[68]</sup>

Electron transfer is fast, while diffusion of small charge-compensating cations into the bulk of materials is slower. For example,

diffusion coefficient of deuterium in ZnO is  $\approx 10$  nm<sup>2</sup> s<sup>-1</sup>.<sup>[129,130]</sup> In case of Li<sup>+</sup> and TiO<sub>2</sub> anatase films the diffusion coefficients range from 0.001 nm<sup>2</sup> s<sup>-1</sup> (7 nm particles)<sup>[126]</sup> up to 10 nm<sup>2</sup> s<sup>-1</sup> (anatase single crystal).<sup>[131]</sup> Therefore transfer of a charge-compensating ion into the bulk of 5 nm particle occurs on the time scale exceeding seconds—much longer than electron transfer. From this standpoint, microporous structure of certain particles,<sup>[132]</sup> MOFs<sup>[48]</sup> and ionic carbon nitrides (Figure 3) improves transport of charge-compensating cations, which results in higher  $R_{PC}$ . In cation containing PHIs, diffusion coefficients for ion motion determined via the Nernst–Einstein equation are  $(50 \pm 7) \times 10^3$  nm<sup>2</sup> s<sup>-1</sup> for Na-PHI and  $(5 \pm 0.7) \times 10^3$  nm<sup>2</sup> s<sup>-1</sup> for K-PHI and Li-PHI suggesting directional ion transport through channels (Figure 3).<sup>[44]</sup> Several orders of magnitude higher diffusivity of ions via micropores compared to slow intercalation of H<sup>+</sup> and Li<sup>+</sup> into the bulk of semiconductor nanoparticles explains enhanced rate of H<sub>2</sub> evolution under continuous illumination<sup>[44,133,134]</sup> and fast electron extraction in PHI-based photoanodes<sup>[135]</sup>—alkali metal ions assist electron transport through the carbon nitride network.

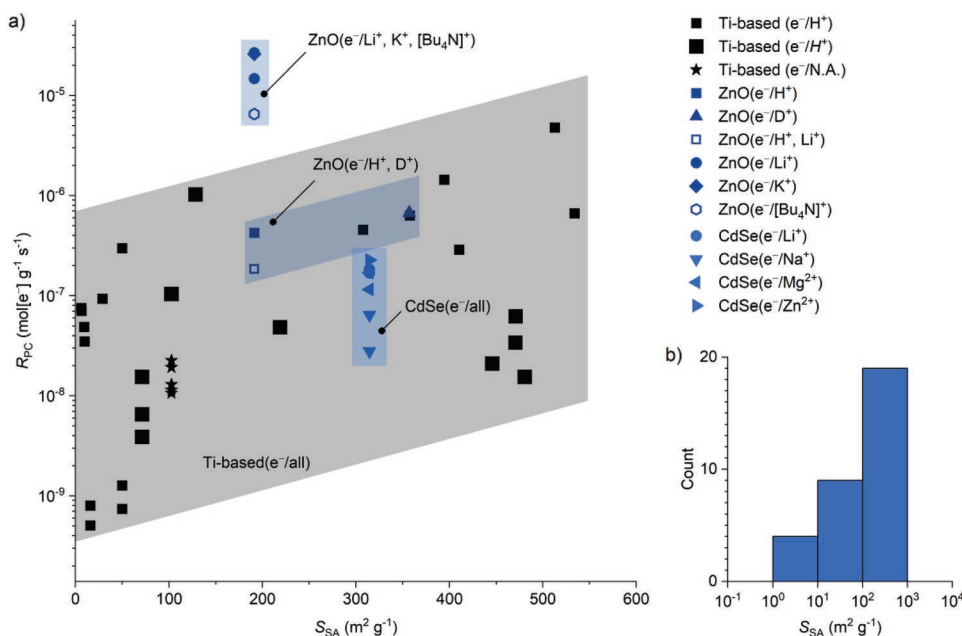


**Figure 17.** Photocharging of SCPs. a) Dependence of  $R_{PC}$  on  $S_{SA}$  plotted in semilogarithmic scale. b) Distribution of the corresponding  $S_{SA}$  values.

## 6.2. Dependence of $R_{PC}$ on Material Specific Surface Area

Considering that electron transfer between SCP and reductant is a surface reaction, specific surface area of materials ( $S_{SA}$ ) may affect  $R_{PC}$ . In Figure 17a  $R_{PC}$  is plotted versus  $S_{SA}$ , while distribution of  $S_{SA}$  values that were either taken from the references or calculated according to Equation (6) is shown in Figure 17b. Majority of materials studied in photocharging have surface area  $>100 \text{ m}^2 \text{g}^{-1}$ . For Ti-based materials,  $R_{PC}$  increases by at least ten times as  $S_{SA}$  changes from  $\approx 10$  to  $500 \text{ m}^2 \text{g}^{-1}$ . The fact that data even for the same class of materials is strongly scattered indicates that high  $S_{SA}$  is not the primary parameter that affects  $R_{PC}$ —materials with large surface are photocharged slowly if conditions are not optimized. For example, at low pH,  $H^+$  readily available in the reaction mixture facilitate fast charging of SCPs.<sup>[124]</sup> Another component that affects  $R_{PC}$  is capping agents, especially those having low oxidation potential (alcohols, amines),<sup>[116]</sup> introduced during synthesis and strongly bound to the surface of the particle. Due to short distance, electron transfer from, in this case sacrificial capping agent to the SCP, is fast. A peculiar example of rather fast charging, is synthesis of  $TiO_2(e^-/H^+)$  particles upon photolysis of titanium(IV)glycolate<sup>[132]</sup>—ligand provides  $e^-/H^+$  to charge  $TiO_2$  during particles growth.

## 6.3. Apparent Quantum Yield of SCPs Photocharging

Like any photochemical process, the efficiency of photocharging can be quantitatively expressed through apparent quantum yield (AQY)—the number of electrons permanently stored in the semiconductor per photon absorbed by the material. The AQY of photocharged Cd-based nanodumbbells—CdSe nanorods decorated with Au nanoparticles, is  $10^{-4} \%$  upon excitation at 532 nm

in 3.4 M aqueous EtOH solution.<sup>[136]</sup> Surface-bound ethoxide groups in  $TiO_2$  sol results in AQY of 3.8% compared to 0.5% for ethoxide-free sol.<sup>[116]</sup> AQY of anatase  $TiO_2(e^-/H^+)$  particles with the diameter 2.4 and 3 nm are 3% and 3.8%, respectively.<sup>[76,78]</sup> AQY of  $TiO_2/Ag(e^-/H^+)$  and  $TiO_2/Au(e^-/H^+)$  hybrid materials are in the range of 3.9–8.8%.<sup>[137]</sup> Kuznetsov et al. reported AQY of photocharged Ti-based gels ranging from tens of percent<sup>[50]</sup> and up to remarkable  $46 \pm 4\%$ .<sup>[75]</sup> Such high AQY values clearly point at high efficiency of the process due to developed microporous structure of gels. On the other hand, Castellano et al. measured AQY of photocharged Ti-based gels to be  $1\% \pm 0.5\%$ .<sup>[52]</sup> In  $TiO_2-WO_3$  hybrid composites,  $TiO_2$  phase harvests photons and serves as the primary reservoir for electron storage. Due to the more positive Fermi level, electrons are transferred from  $TiO_2$  to  $WO_3$ . Ngaotrakanwivat and Tatsuma found that by increasing the  $WO_3:TiO_2$  ratio in the hybrid composite film from 0.2 to 0.5 the AQY increases from  $2.8\% \pm 0.7\%$  to  $5.4\% \pm 0.3\%$ , which they ascribed to shorter path for electron injection from  $TiO_2$  into  $WO_3$  – the probability of  $e^-/h^+$  recombination decreases.<sup>[138]</sup> Further improvement of AQY was achieved by increasing film thickness to harvest all incident photons. Decreasing light intensity was necessary to reach higher AQY, since at higher photon flux intercalation of  $H^+$  rather than photon absorption becomes a rate-limiting step. Since  $TiO_2-WO_3$  hybrid composites use water vapor as donor of electrons and protons, increasing air humidity gives higher AQY.

## 7. Electron Storage

### 7.1. Dependence of $\delta_{max}$ on SCP Volume

Using a series of ZnO nanoparticles, Schimpf et al. proved that  $N_{max}$  in  $ZnO(e^-/Li^+)$  is independent within the range of

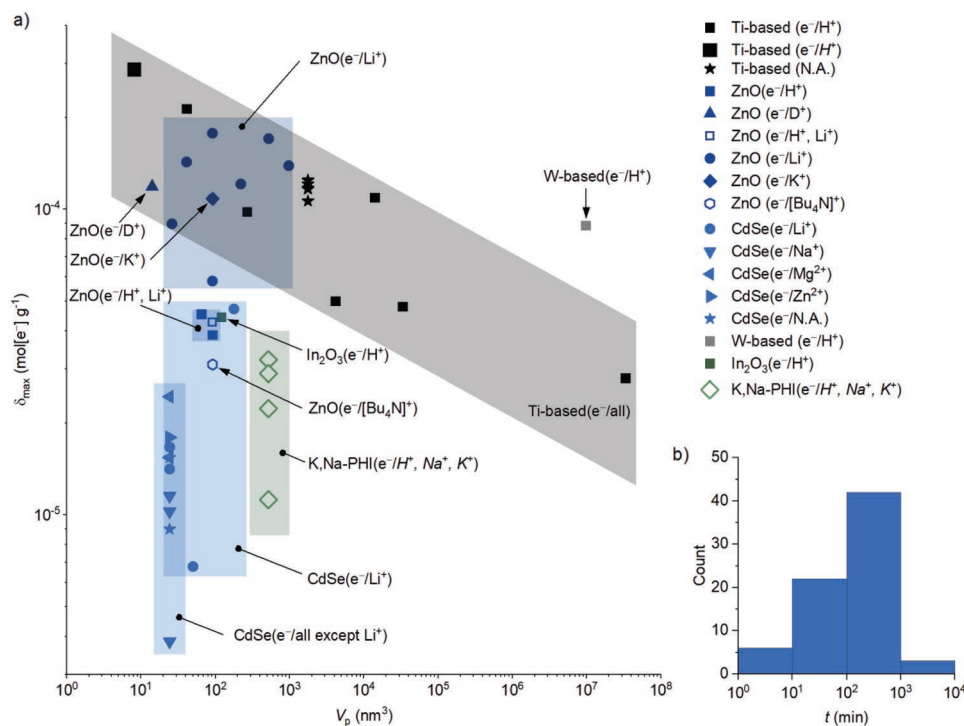


**Figure 18.** Electron storage in SCPs. a) Dependence of  $\delta_{\max}$  on  $V_p$  in logarithmic scale. Subscript “max” in Y-axis label indicates that saturation of the SCP with electrons was achieved. b) Distribution of the corresponding photolysis times.

particles radii  $r = 1.5\text{--}6$  nm.<sup>[64]</sup> As inferred from Equation (8)  $\delta_{\max}$  scales linearly with  $N_{\max}$ . Therefore,  $\delta_{\max}$  is nearly constant,  $(13 \pm 4) \times 10^{-5}$  mol[e<sup>-</sup>] g<sup>-1</sup>, for the given range of  $V_p$  as shown in **Figure 18** (dark blue circles). Three times higher  $\delta_{\max}$  values are obtained for ZnO(e<sup>-</sup>/M<sup>+</sup>) using Li-, K-borohydrides, as electron donors,  $(12 \pm 4) \times 10^{-5}$  mol[e<sup>-</sup>] g<sup>-1</sup>, compared to EtOH or a mixture of EtOH/Li[PF<sub>6</sub>],  $(4 \pm 0.3) \times 10^{-5}$  mol[e<sup>-</sup>] g<sup>-1</sup>. On the other hand, Faucheaux and Jain photocharged ZnO in MeOH-d<sub>4</sub> to  $12 \times 10^{-5}$  mol[e<sup>-</sup>] g<sup>-1</sup>,<sup>[119]</sup> which is comparable to the experiment with metal borohydrides. Photocharging of ZnO in the presence of [Bu<sub>4</sub>N][Et<sub>3</sub>BH] gave ZnO(e<sup>-</sup>/[Bu<sub>4</sub>N]<sup>+</sup>) with concentration of electrons comparable to that using EtOH, which underlines the importance of counter ion—small cation can intercalate into the bulk of ZnO, while [Bu<sub>4</sub>N]<sup>+</sup> are stored on the surface. Therefore, [Bu<sub>4</sub>N]<sup>+</sup> can stabilize only relatively few electrons in nonporous ZnO. Optimum  $\delta_{\max}$  of  $3.2 \times 10^{-5}$  mol[e<sup>-</sup>] g<sup>-1</sup> for K,Na-PHI (e<sup>-</sup>/H<sup>+</sup>, Na<sup>+</sup>, K<sup>+</sup>) was achieved at  $C_{ED}(\text{MeOH})$  2.48 mol L<sup>-1</sup>.<sup>[139]</sup> CdSe nanoparticles are photoreduced in the presence of metal borohydrides and organometallic reductants to  $\delta_{\max}$   $(1.7 \pm 1.2) \times 10^{-5}$  mol[e<sup>-</sup>] g<sup>-1</sup>.<sup>[90]</sup> W-based TiO<sub>2</sub>-WO<sub>3</sub> hybrid composite can accumulate  $9 \times 10^{-5}$  mol[e<sup>-</sup>] g<sup>-1</sup>.<sup>[140]</sup> Despite electrons are initially accumulated in TiO<sub>2</sub>, due to the more positive Fermi level in WO<sub>3</sub> compared to TiO<sub>2</sub>, e<sup>-</sup>/H<sup>+</sup> are transferred into WO<sub>3</sub> and stored in tungsten bronze (H<sub>x</sub>WO<sub>(3-x)</sub>). In<sub>2</sub>O<sub>3</sub> nanoparticles with the diameter of 6.15 nm are photocharged up to  $4.4 \times 10^{-5}$  mol[e<sup>-</sup>] g<sup>-1</sup>.<sup>[112]</sup> In TiO<sub>2</sub>,  $\delta_{\max}$  decreases from  $\approx 29 \times 10^{-5}$  to  $\approx 2.8 \times 10^{-5}$  mol[e<sup>-</sup>] g<sup>-1</sup> when  $V_p$  changes from 8 nm<sup>3</sup> ( $d = 2.5$  nm assuming spherical shape) to  $3 \times 10^7$  nm<sup>3</sup> ( $d = 400$  nm).<sup>[67]</sup> On the one hand low sensitivity of  $\delta_{\max}$  on  $V_p$  for Ti-based semiconductors (gray area in **Figure 18**) could be rationalized by variation in experimental conditions used in reference articles—in other

words, similar to ZnO nanoparticles,<sup>[64]</sup>  $\delta_{\max}$  does not depend on particle diameter. On the other hand at particle  $d \approx 400$  nm intercalation of H<sup>+</sup> into the bulk of metal oxides becomes a rate limiting step (see also Section 6.1). At relatively short photolysis experiment (minutes, **Figure 18b**), charge-compensating ions, such as H<sup>+</sup>, Li<sup>+</sup>, are likely to be stored in subsurface region, while their homogenization by diffusion into the bulk occurs at much longer time scale, hours. Diffusion of e<sup>-</sup>/H<sup>+</sup> deeper into the bulk of several hundreds nm large microporous NCN-CN<sub>x</sub> and K-PHI particles might be responsible for decrease of H<sub>2</sub> amount evolved upon subsequent addition of Pt-catalyst in dark.<sup>[34,38]</sup>

When SCP(e<sup>-</sup>/H<sup>+</sup>) is brought in contact with transition metal particle, such as Au or Ag,<sup>[51,136,137,141]</sup> equilibration of the Fermi levels in these materials takes place—electrons migrate from SCP(e<sup>-</sup>/H<sup>+</sup>) to the metal nanoparticle. Up to twice higher  $\delta$  values were obtained for a hybrid composite made of 22.5 nm TiO<sub>2</sub> ( $C_{SCP} = 13 \times 10^{-6}$  M) and 5 nm Au particles ( $0.11$  or  $0.16 \times 10^{-6}$  M) compared to TiO<sub>2</sub> nanoparticles of the same diameter and photocharged under the same conditions.<sup>[51,142]</sup> As  $\delta$  depends on gravimetric density of a composite, at high content of metal nanoparticles  $\delta_{\max}$  naturally decreases.<sup>[137,142]</sup> Being conductive single-walled carbon nanotubes (SWCNTs) can be used instead of metal nanoparticles in hybrid composites with SCPs.<sup>[81]</sup> Due to lower gravimetric density of SWCNTs compared to transition metal particles, higher  $\delta_{\max}$  values are expected. However, Kongkanand and Kamat showed that in SWCNT one electron is stored per  $\approx 100$  carbon atoms<sup>[143]</sup> which is 5–20 times lower compared to TiO<sub>2</sub>. Therefore,  $\delta_{\max}$  is reversibly proportional to the content of SWCNTs in the composite.

Small organic molecules capable to undergo facile PCET from photocharged SCP(e<sup>-</sup>/H<sup>+</sup>) naturally affect  $\delta_{\max}$ . For example,  $\delta_{\max}$

values for TiO<sub>2</sub> nanoparticles photocharged in the presence of 20 × 10<sup>-3</sup> and 80 × 10<sup>-3</sup> M styrene oxide are three and six times lower compared to photocharging of TiO<sub>2</sub> in the absence of styrene oxide.<sup>[113]</sup> Similarly, δ<sub>max</sub> values for ZnO nanoparticles (d = 3.8 and 7.4 nm) decrease linearly with the concentration of added acetaldehyde.<sup>[14]</sup> These two examples clearly indicate that despite styrene oxide and acetaldehyde serve as electron acceptors, they do not suppress completely photocharging of semiconductors. Instead equilibrium between oxidized (acetaldehyde or styrene oxide) and reduced (ethanol or styrene) forms of the molecule is established and accompanied by partial discharging of the SCP. These examples also signify that impurities or additives may be responsible, at least partially, for data points scattering in Figure 18a.

## 7.2. Dependence of ⟨n<sub>max</sub>⟩ on SCP Volume

Schimpf et al. found that ⟨n<sub>max</sub>⟩ for ZnO nanoparticles with radii in the range r = 1.5–6 nm scales linearly with r<sup>3</sup>.<sup>[64]</sup> Data shown in Figure 19 confirm that such trend is also valid for several classes of materials in the range of diameters from 1 to 400 nm. The data are scattered with respect to the trend line, which again indicates that there are properties of the materials, particles as well as photocharging conditions that influence ⟨n<sub>max</sub>⟩.

## 7.3. Dependence of R<sub>PC</sub> on δ<sub>max</sub>

lorio et al. noted that initial rate of photocharging correlates with the maximum concentration of electrons that TiO<sub>2</sub>(e<sup>-</sup>/H<sup>+</sup>)

sol can store.<sup>[116]</sup> As shown in Figure 20, similar trend is also valid for several classes of materials. More important, when conditions of SCPs photocharging such as semiconductor type, electron donor, counter ion, are kept the same, for Ti-based particles in the range of d = 0.95–21 nm and TiO<sub>2</sub>(WO<sub>3</sub>) hybrid composites, R<sub>PC</sub> scales linearly with δ<sub>max</sub> as indicated by trend lines in Figure 20.<sup>[68,81,113,114,116]</sup> Given that accumulation of electrons is accompanied by intercalation of H<sup>+</sup> or other structural changes to maintain electric neutrality, the rate of this process matches the rate of electrons accumulation, at least for 0.95–21 nm particles. Slope of the fitting lines may be considered as sensitivity of R<sub>PC</sub> change versus δ<sub>max</sub> and for given set of materials is in the range (1.8–62) × 10<sup>-4</sup> s<sup>-1</sup>. More precise analysis of slope values is hampered by substantial variation in experimental conditions. For example, in Figure 20 data that were fitted with dark green dashed line was acquired for anatase TiO<sub>2</sub> sol (crystallite d = 3.7 and 3.9 nm) photocharged in ethanol:water:HCl mixture (16.2:2.8:0.040 M), while data fitted with light green dashed line— for anatase:rutile (80:20) TiO<sub>2</sub> (d = 21 nm) particles in pure iso-propanol.<sup>[113]</sup> A full factorial experiment could potentially rationalize the sensitivity of R<sub>PC</sub> change versus δ<sub>max</sub>.

## 8. Discharging of SCP(e<sup>-</sup>/X<sup>+</sup>) in Dark

### 8.1. Dependence of R<sub>DC</sub> on V<sub>p</sub>

Similar to photocharging, R<sub>DC</sub> decrease when particles become larger, which once again underlines the fact that discharging is a surface process (Figure 21). Saouma et al. studied discharging

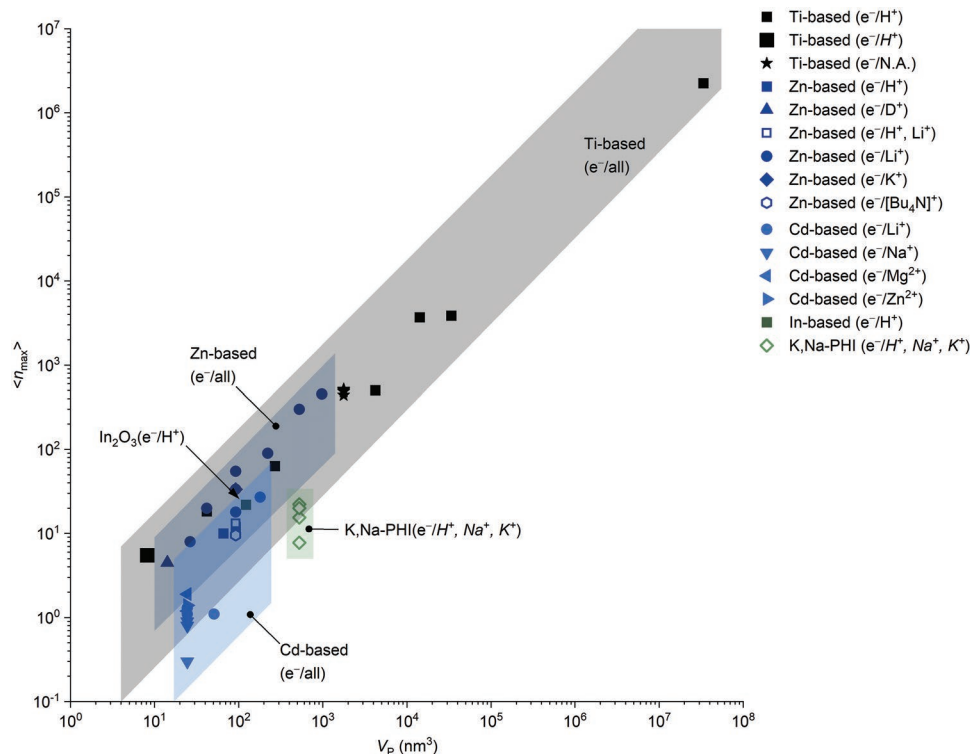
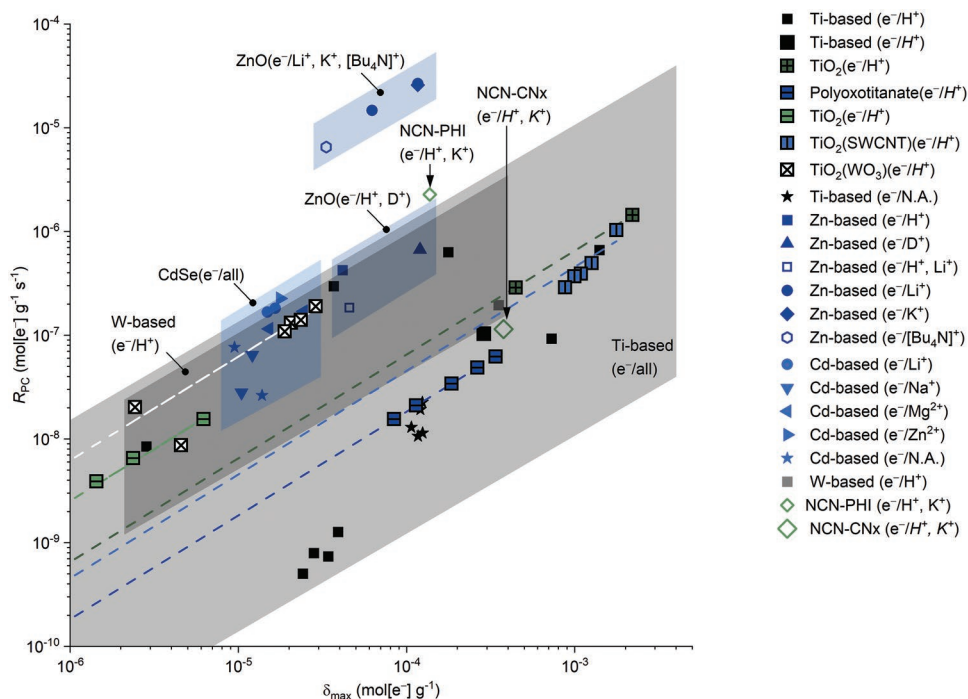


Figure 19. Dependence of ⟨n<sub>max</sub>⟩ on V<sub>p</sub> in logarithmic scale. Subscript “max” in Y-axis label indicates that saturation of the SCP with electrons was achieved.





**Figure 20.** Dependence of  $R_{PC}$  on  $\delta_{max}$ . Dark green dashed line –  $TiO_2(e^-/H^+)$ ,<sup>[116]</sup> dark blue dashed line – polyoxotitanate( $e^-/H^+$ ),<sup>[68]</sup> light green dashed line –  $TiO_2(e^-/H^+)$ ,<sup>[113]</sup> light blue dashed line –  $TiO_2(SWCNT)(e^-/H^+)$ ,<sup>[81]</sup> and white dashed line –  $TiO_2(WO_3)(e^-/H^+)$ .<sup>[114]</sup>

of  $\approx 700$  nm MIL-125( $e^-/H^+$ ) particles by  ${}^tBu_3ArO^+$ .<sup>[45]</sup> Despite much larger diameter, MIL-125 shows  $R_{DC}$  comparable to 15–21 nm anatase or anatase:rutile  $TiO_2$  particles,<sup>[77,144]</sup> which is due to microporous structure of the MOF that facilitates transport of  $e^-/H^+$ . While  $e^-/H^+$  are stored in bulk, reduction of  ${}^tBu_3ArO^+$  occurs on the surface as the latter is too large to enter MOF pore.

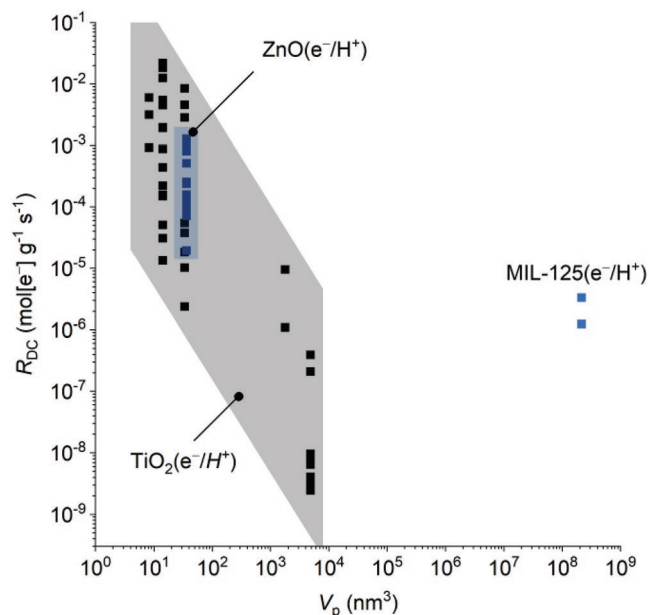


**Figure 21.** Discharging of SCP( $e^-/H^+$ ) in dark. Dependence of  $R_{DC}$  on  $V_p$ .

## 8.2. Dependence of $R_{DC}$ on Initial Concentration of Electrons in SCP

As discussed in Section 2.3, in electronically doped SCPs the Fermi level is shifted upward as more and more electrons are added to the SCP. As a result, stronger driving force for electron transfer is created as deduced from Equation (1)—therein  $E_{CB}$  should be replaced by the Fermi level. Indeed,  $R_{DC}$  scales linearly with  $\delta$  for several classes of materials (Figure 22). Such conclusion is valid for  $NCN-CN_x(e^-/H^+, K^+)$ <sup>[34]</sup> and  $H-PHI(e^-/H^+, K^+)$ <sup>[38]</sup> discharged upon addition of Pt nanoparticles in dark; 4.1 nm  $ZnO(e^-/H^+)$  particles discharged with TEMPO ( $2.4 \times 10^{-3}$  M);<sup>[129]</sup> 21 nm anatase:rutile (80:20)  $TiO_2(e^-/H^+)$  particles discharged with styrene oxide ( $20 \times 10^{-3}$  M).<sup>[113]</sup> On the other hand, in redox-shifted SCPs, the Fermi level remains constant, while increase of  $R_{DC}$  with  $\delta$  may be rationalized assuming that discharging obeys second-order kinetics—velocity is proportional to the product of electrons concentration in SCP( $e^-/X^+$ ) and  $C_{EA}$  (see Section 8.3 for specific electron acceptors).<sup>[78,122,145]</sup> Therefore, whether SCPs are electronically doped or redox-shifted, under otherwise identical conditions those photocharged to a greater extent will transfer electrons faster. Slope of fitting lines shown in Figure 22 reflect sensitivity of  $R_{DC}$  to concentration of electrons in SCP( $e^-/X^+$ ).  $R_{DC}$  values for discharging of  $ZnO(e^-/H^+)$  particles with TEMPO are the most sensitive to change in  $\delta$ , with the slope equal to  $34$  s<sup>-1</sup>, followed by  $TiO_2(e^-/H^+)$  particles (slope  $2 \times 10^{-3}$  s<sup>-1</sup>) and ionic carbon nitrides (slope  $2 \times 10^{-4}$  s<sup>-1</sup>). Due to different structure of materials, particles diameter, oxidant, and other experimental conditions at this point it is difficult to explain the observed dependence. Similar to trends noted in Figure 20, full factorial experiment might be useful in this case as well.

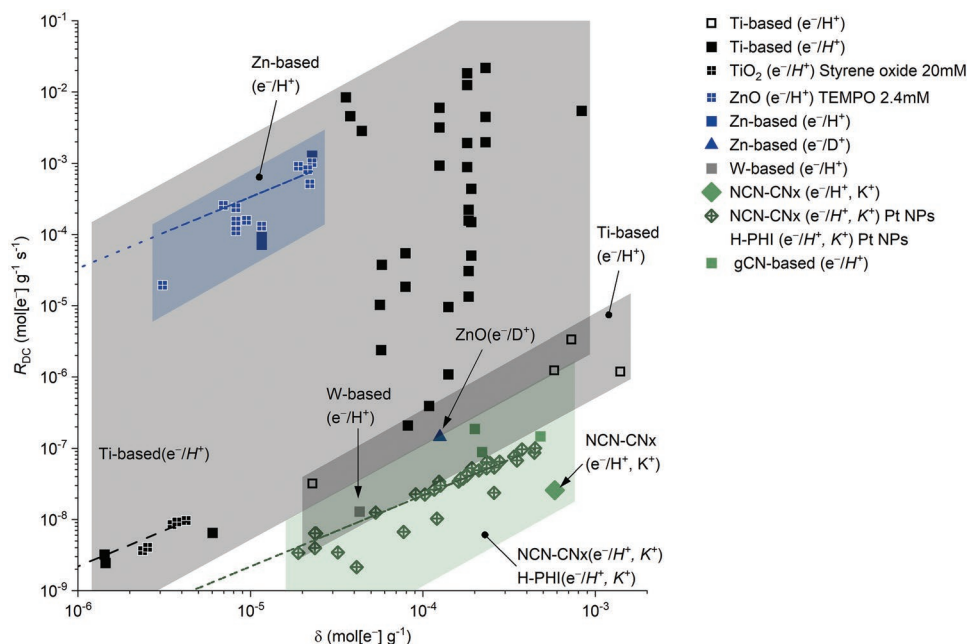


**Figure 22.** Dependence of  $R_{DC}$  on  $\delta$ . Green dashed fitting line – NCN-CNx( $e^-/H^+$ ,  $K^+$ )<sup>[34]</sup> and H-PHI( $e^-/H^+$ ,  $K^+$ )<sup>[38]</sup> discharged upon addition of Pt nanoparticles in dark; blue dashed fitting line – 4.1 nm ZnO( $e^-/H^+$ ) particles discharged with TEMPO ( $2.4 \times 10^{-3}$  M);<sup>[129]</sup> black dashed fitting line – 21 nm TiO<sub>2</sub>( $e^-/H^+$ ) particles discharged with styrene oxide ( $20 \times 10^{-3}$  M).<sup>[113]</sup>

### 8.3. Dependence of $R_{DC}$ on $C_{EA}$

As shown in **Figure 23**, for TiO<sub>2</sub> particles with  $d = 2.5\text{--}4$  nm,<sup>[78,122,145]</sup>  $R_{DC}$  increases with  $C_{EA}$ , while it is 4–7 orders of magnitude lower for SCPs with  $d = 21$  nm,<sup>[113]</sup> which might again be explained by longer time required for H<sup>+</sup> to diffuse from the bulk to the surface of relatively large nonporous TiO<sub>2</sub> particles. Microporous structure of MOF MIL-125, on the

other hand, facilitates faster transport of  $e^-/H^+$  from the bulk to the surface of the material—despite substantially larger diameter of MIL-125 particles,  $R_{DC}$  in this case is only 1–4 orders of magnitude lower compared to 2.5–4 nm TiO<sub>2</sub> particles.<sup>[45]</sup> Data shown in **Figure 23** were acquired using various oxidants.

Braten et al. found that  $R_{DC}$  of ZnO( $e^-/H^+$ ) increases ten times when TEMPO concentration is changed from  $0.12 \times 10^{-3}$  to  $2.4 \times 10^{-3}$  M.<sup>[129]</sup> Using a large set of electron acceptors,

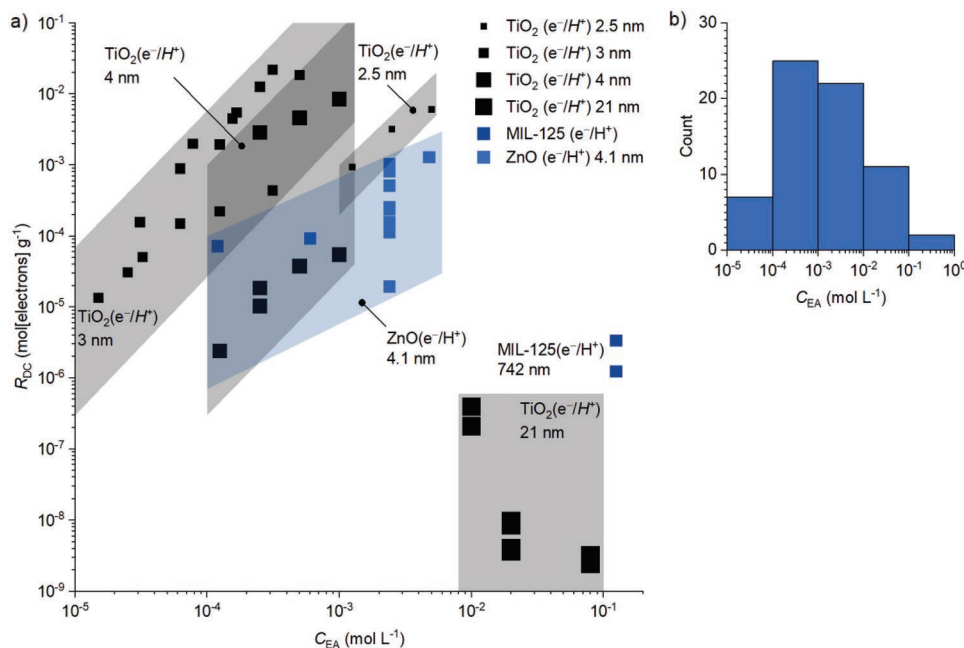


**Figure 23.** Discharging of SCPs. a) Dependence of  $R_{DC}$  on  $C_{EA}$ . b) Distribution of  $C_{EA}$ .

O<sub>2</sub>, H<sub>2</sub>O<sub>2</sub>, and NO<sub>3</sub><sup>-</sup> anion;<sup>[78]</sup> CuCl<sub>2</sub>;<sup>[78]</sup> AgClO<sub>4</sub>;<sup>[145]</sup> HgCl<sub>2</sub>, PbCl<sub>2</sub>, NiCl<sub>2</sub><sup>[122]</sup> in combination with stopped-flow technique, Mohamed et al. found that quenching of TiO<sub>2</sub>(e<sup>-</sup>/H<sup>+</sup>) follows second-order kinetics when electrons in the semiconductor are present in excess compared to the electron acceptor. This aspect is discussed in detail in Section 8.4.

#### 8.4. Dependence of $k_{DC}$ on Reduction Potential of Electron Acceptors

Without doubts laser flash photolysis (LFP) is a powerful technique to determine rate constant of electron transfer between SCPs and electron acceptors.<sup>[146]</sup> However, LFP generates one hole–electron pair per nanoparticle, which is significantly smaller number compared to  $\langle n_{max} \rangle$ , tens and hundreds of electrons typically achievable for SCP(e<sup>-</sup>/H<sup>+</sup>) (Figure 19), which taking into account dependence of  $R_{DC}$  on  $\delta$  could give lower rates.<sup>[78]</sup> On the other hand, coordination of electron acceptors to SCP might give higher rate of electron transfer in LFP experiment compared to data obtained using stopped-flow technique and SCP(e<sup>-</sup>/H<sup>+</sup>). For example, bimolecular rate constant ( $k_{DC}$ ) of electron transfer from TiO<sub>2</sub>(e<sup>-</sup>/H<sup>+</sup>) to O<sub>2</sub> was determined to be  $7.6 \times 10^7 \text{ M}^{-1} \text{ s}^{-1}$ ,<sup>[147]</sup> which is three orders of magnitude faster than quenching with O<sub>2</sub> of 3 nm TiO<sub>2</sub>(e<sup>-</sup>/H<sup>+</sup>) photocharged to  $\langle n \rangle = 6e^-$  in a stopped-flow experiment.<sup>[78]</sup> On the other hand, in stopped-flow experiments methylviologen oxidizes 4.1 nm ZnO(e<sup>-</sup>/H<sup>+</sup>) photocharged to less than 1e<sup>-</sup> per particle with  $k_{DC} > 10^7 \text{ M}^{-1} \text{ s}^{-1}$ ,<sup>[83]</sup> while TiO<sub>2</sub>(e<sup>-</sup>/H<sup>+</sup>) generated in situ during LFP experiment is oxidized by methylviologen with comparable  $k_{DC} = (4.5 \pm 0.6) \times 10^7 \text{ M}^{-1} \text{ s}^{-1}$ .<sup>[65]</sup> This review focuses on application of photocharged materials as reductants in dark. Therefore, in this section only bimolecular rate constants of SCP(e<sup>-</sup>/H<sup>+</sup>) discharging in dark ( $k_{DC}$ ) obtained from stopped-flow experiments will be analyzed. Obare et al. determined  $k_{DC}$  between TiO<sub>2</sub>(e<sup>-</sup>/H<sup>+</sup>) or TiO<sub>2</sub>(e<sup>-</sup>/H<sup>+</sup>) loaded with heme and organohalides.<sup>[144]</sup> Mohamed et al. correlated  $\log_{10}(k_{DC})$  with the driving force of electron transfer, which is defined by the difference between the reduction potential of the transition metal cation ( $E_{red}$ , V vs NHE) and CB potential in TiO<sub>2</sub> (-0.5 V vs NHE).<sup>[122]</sup> The data from several sources are plotted in Figure 24.

Quenching of TiO<sub>2</sub>(e<sup>-</sup>/H<sup>+</sup>) proceeds faster when stronger oxidants are employed, which is consistent with stronger driving force of the process (Equation (3)). In quantitative terms, electron transfer rate constants cover a range of  $\approx 10^7$  when the driving force changes over the range of 3.3 V.

### 9. Application of Photocharged Materials for Reduction of Organic Compounds

In electronically doped SCPs (Figure 8a), addition of the first electron results in more pronounced shift of the Fermi level compared to addition of the second, third, and all subsequent electrons.<sup>[14]</sup> Assuming that SCP(e<sup>-</sup>/H<sup>+</sup>) is fully charged, in a reversed process transfer of few electrons from the SCP(e<sup>-</sup>/H<sup>+</sup>) to a substrate reduces the Fermi level only slightly. In other words, SCP(e<sup>-</sup>/H<sup>+</sup>) can provide several equivalents of electrons at nearly the same potential.<sup>[96]</sup> It is a great advantage compared to, for example, small redox sensitizers that mediate

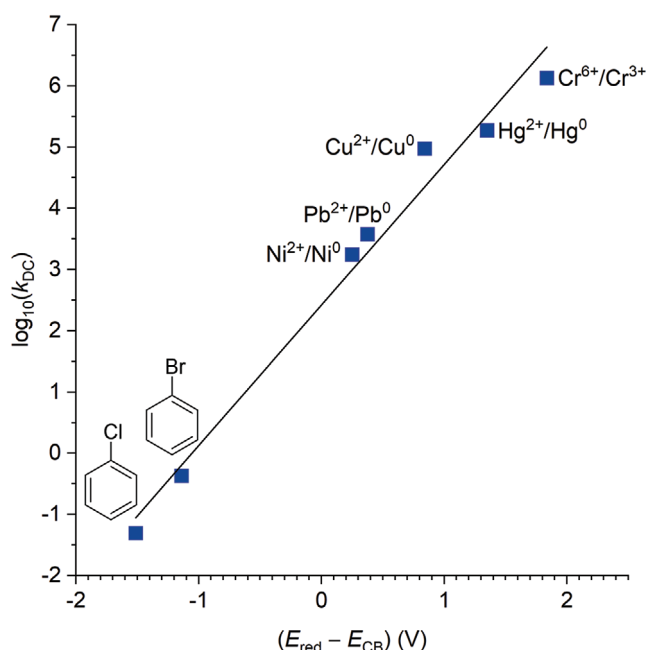


**Figure 24.** Dependence of  $\log_{10}(k_{DC})$  on the driving force of electron transfer ( $E_{red} - E_{CB}$ ) from photocharged TiO<sub>2</sub>(e<sup>-</sup>/H<sup>+</sup>) to various oxidants. Reduction potentials were converted to NHE scale according to relations discussed by Pavlishchuk and Addison.<sup>[148]</sup> Bimolecular rate constants  $k_{DC}$  and reduction potentials of oxidants are taken from the references: chlorobenzene  $k_{DC} = 0.05 \text{ M}^{-1} \text{ s}^{-1}$ ,<sup>[144]</sup>  $E_{red} = -2.014 \text{ V}$ ;<sup>[149]</sup> bromobenzene  $k_{DC} = 0.43 \text{ M}^{-1} \text{ s}^{-1}$ ,<sup>[144]</sup>  $E_{red} = -1.64 \text{ V}$ ;<sup>[149]</sup> Ni<sup>2+</sup>  $k_{DC} = 1.77 \times 10^3 \text{ M}^{-1} \text{ s}^{-1}$ ,  $E_{red} = -0.25 \text{ V}$ ;<sup>[122]</sup> Pb<sup>2+</sup>  $k_{DC} = 3.8 \times 10^3 \text{ M}^{-1} \text{ s}^{-1}$ ,  $E_{red} = -0.126$ ;<sup>[122]</sup> Cu<sup>2+</sup>  $k_{DC} = 9.4 \times 10^4 \text{ M}^{-1} \text{ s}^{-1}$ ,<sup>[78]</sup>  $E_{red} = 0.34 \text{ V}$ ;<sup>[122]</sup> Hg<sup>2+</sup>  $k_{DC} = 1.89 \times 10^5 \text{ M}^{-1} \text{ s}^{-1}$ ,<sup>[122]</sup>  $E_{red} = 0.85 \text{ V}$ ;<sup>[122]</sup> Cr<sup>6+</sup>  $k_{DC} = 1.34 \times 10^6 \text{ M}^{-1} \text{ s}^{-1}$ ,<sup>[150]</sup>  $E_{red} = 1.336 \text{ V}$ .

single electron transfer (SET) and not multielectron transfer. Results of several groups unambiguously point at the ability of SCP(e<sup>-</sup>/H<sup>+</sup>) to transfer from 1 to 6 electrons and protons per substrate molecule. The reactivity pattern depends on structure of SCP(e<sup>-</sup>/H<sup>+</sup>) and intrinsic reactivity of substrates engaged in the reaction.

#### 9.1. Transfer of 1e<sup>-</sup>/1H<sup>+</sup>

Mechanism of photoredox reactions mediated by molecular sensitizers, organic dyes, and transition metal complexes, is explained in terms of SET.<sup>[6]</sup> SCP having slight excess of electrons under continuous illumination or SCP(e<sup>-</sup>/H<sup>+</sup>) carrying large excess of electrons in dark can also mediate 1e<sup>-</sup>/1H<sup>+</sup> reactions, especially if they yield thermodynamically stable products. These reactions typically proceed via PCET rather than stepwise transfer of electron and proton.<sup>[65]</sup> Notable examples are reduction of alkoxy and N-oxyl radicals, <sup>t</sup>Bu<sub>3</sub>ArO<sup>•</sup> and TEMPO—they are converted into phenol and N-hydroxylamine, respectively (Figure 25a).

Synthetically more useful reaction is generation of ketyl radical from enone **1a** (Figure 25b).<sup>[151]</sup> Addition of a ketyl radical to the starting enone **1a** followed by HAT/PCET and elimination of H<sub>2</sub>O yields substituted hexadienone **2a**.<sup>[36]</sup> Kurpil and Savateev found that under continuous illumination using

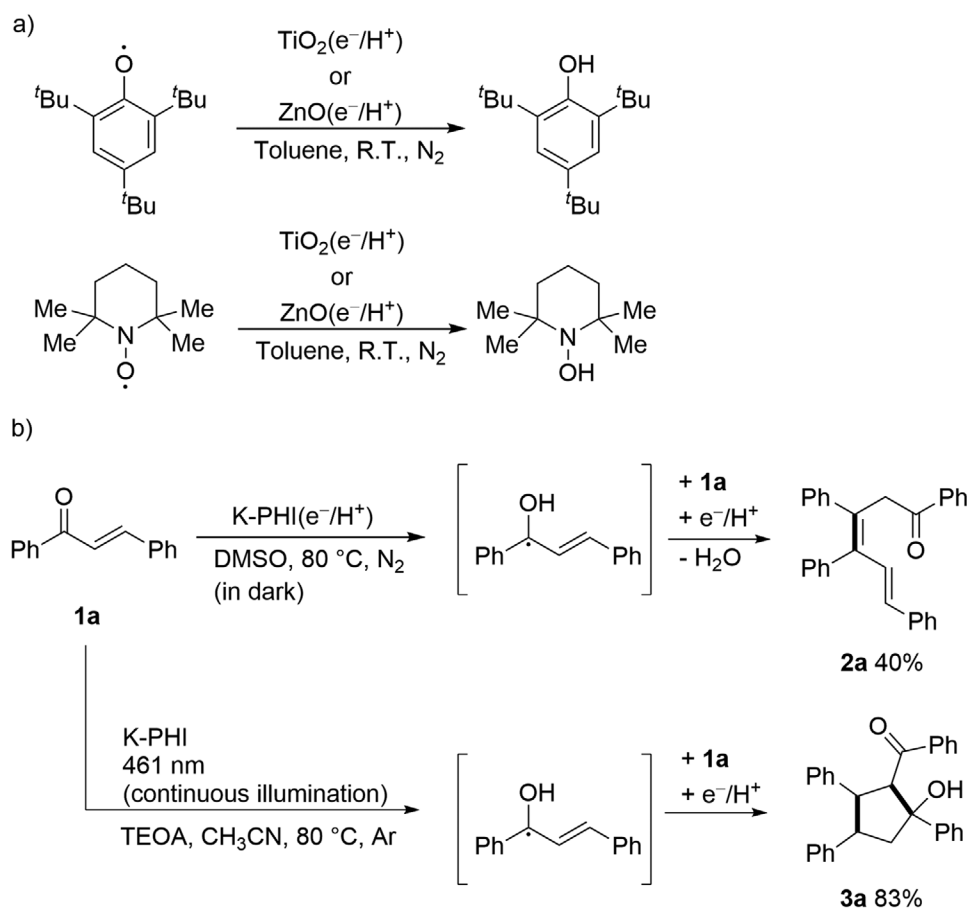


**Figure 25.** PCET reactions from SCP( $e^-/H^+$ ) that involve transfer of  $1e^-/1H^+$ .

triethanolamine as electron donor, selectivity is shifted to cyclopentanol **3a** as the major product.<sup>[151]</sup> PCET mechanism for ketyl radical formation was concluded taking into account CB potential of K-PHI ( $-0.75$  V vs SCE),<sup>[152]</sup> which is not sufficiently negative to reduce enone **1a** to its radical anion via electron transfer ( $E_{1/2} = -1.4$  V vs SCE).<sup>[151]</sup> However, transfer of an electron becomes feasible when coupled with a proton as it avoids formation of highly energetic intermediate—the radical anion. BDFE values instead of redox potentials are used to evaluate thermodynamics of PCET reactions. H–O BDFE in ketyl radicals is only  $\approx 26\text{--}30$  kcal mol $^{-1}$ ,<sup>[102]</sup> which means that electrons and protons are bound to K-PHI( $e^-/H^+$ ) only weakly.

## 9.2. Transfer of $2e^-/2H^+$

Electrons and protons stored in photocharged SCP( $e^-/H^+$ ) do not recombine spontaneously to form  $H_2$ . Catalyst, Pt nanoparticles,<sup>[34,38,153]</sup> MoS $_2$  nanosheets<sup>[117]</sup> or molecular Ni-complex,<sup>[13]</sup> are required to enable evolution of  $H_2$  in dark (**Figure 26a**). 80% of electrons and protons could be harvested from the photocharged amorphous TiO $_2$ ( $e^-/H^+$ ) particles in dark.<sup>[117]</sup>

TiO $_2$ ( $e^-/H^+$ ) and a hybrid composite, heme/TiO $_2$ ( $e^-/H^+$ ), prepared by immobilizing  $\approx 50$  heme molecules at  $\approx 15$  nm TiO $_2$  particle and photocharged in the presence of MeOH reduce aryl halides (**Figure 26b**).<sup>[144]</sup> Experiment with radical clock,

6-bromo-1-hexene, suggests that the reaction proceeds via multi-electron transfer. Mazzanti et al. studied reduction of arylhalides, in particular halogenated aromatic aldehydes and ketones, by K-PHI( $e^-/H^+$ ) (**Figure 26b**).<sup>[36]</sup> Despite presence of C–Br and C=O moieties in substrates that have similar reduction potential ( $E_{1/2} = -1.7$  to  $-1.95$  V vs SCE, respectively), K-PHI( $e^-/H^+$ ) cleaves selectively C–Br bond. Taking into account amount of arylhalide, amount of K-PHI, and the fact that K-PHI can be photocharged up to at least 1 mmol[e $^-$ ] g $^{-1}$ ,<sup>[35]</sup> the efficacy of electrons harvesting in dark was estimated to be  $\approx 60\%$ . K-PHI( $e^-/H^+$ ) retains  $\approx 50\%$  of electrons available for reduction of arylhalides in dark upon storage at  $-25$  °C for 7 days. These results and results obtained by Lotsch and co-workers who found that the amount of  $H_2$  that H-PHI( $e^-/H^+$ ) and NCN-CNx( $e^-/H^+$ ) can release upon addition of Pt nanoparticles in dark decreases after storage of the materials for several hours at room temperature,<sup>[34,38]</sup> suggest that electrons might adopt thermodynamically more stable, less reactive, trap states in the bulk of the materials. Indeed, reactions that involve transfer of  $1e^-/1H^+$  to  $\alpha,\beta$ -unsaturated ketones (**Figure 25b**),<sup>[151,154]</sup> and  $2e^-/2H^+$  transfer reactions (**Figure 26b**) proceed faster when conducted at 80 °C compared to room temperature,<sup>[36]</sup> which point at the kinetic control of  $e^-/H^+$  extraction from the micropores of K-PHI.

Castillo-Lora et al. studied transfer of  $2e^-/2H^+$  from TiO $_2$ ( $e^-/H^+$ ) and ZnO( $e^-/H^+$ ) to *p*-benzoquinone, azobenzene, phenazine, and enamine (**Figure 26c**).<sup>[96]</sup> Hydroquinone,

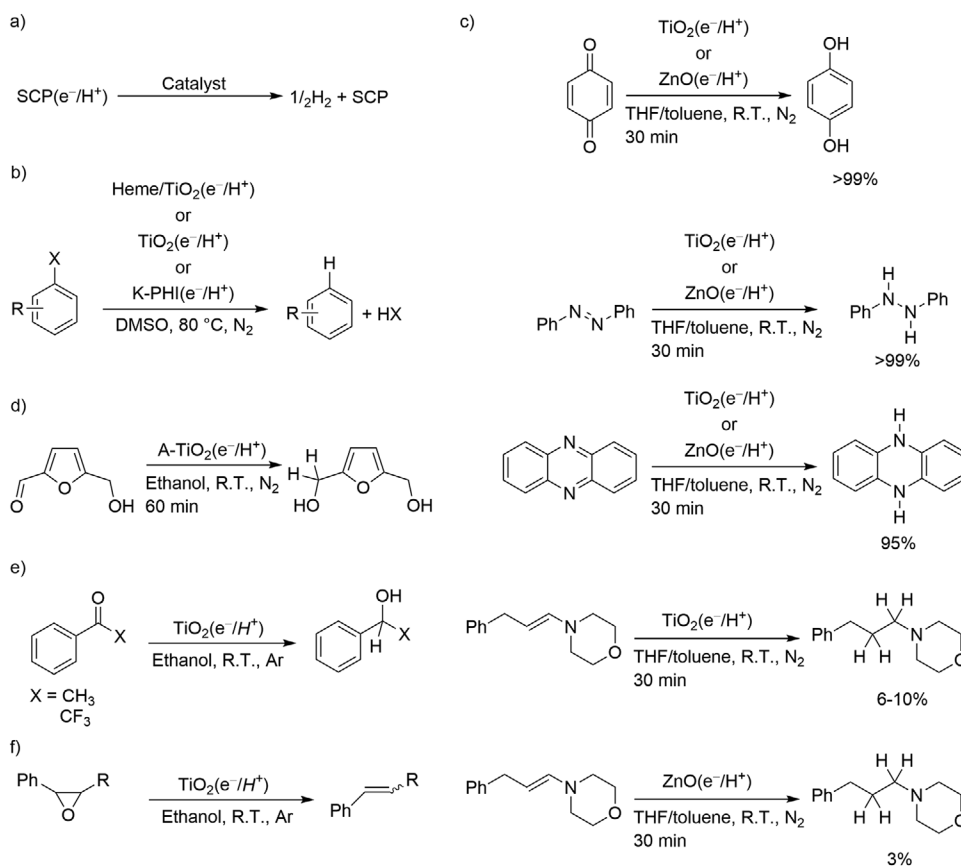


**Figure 26.** PCET reactions from  $\text{SCP}(e^-/H^+)$  that involve transfer of  $2e^-/2H^+$ .

1,2-diphenylhydrazine and 5,10-dihydrophenazine were obtained in >95% yield within 30 min, while conversion of enamine was <10%. Taking into account X–H BDFE values in reduced substrates, upper limit of hydrogen bonding in  $\text{TiO}_2(e^-/H^+)$  and  $\text{ZnO}(e^-/H^+)$  was estimated to be  $\approx 59 \text{ kcal mol}^{-1}$ . Despite 9,10-dihydroanthracene—the product of anthracene  $2e^-/2H^+$  reduction—has BDFE comparable to that in phenylpropylmorpholine,  $56 \text{ kcal mol}^{-1}$ , it is not reduced at significant rate, which implies kinetic effect. Interaction of a substrate with the surface of  $\text{SCP}(e^-/H^+)$  via hydrogen bonding is essential for PCET to proceed. Qiao et al. applied  $e^-/H^+$  stored in amorphous  $\text{TiO}_2$  to reduce 5-hydroxymethylfurfural to 2,5-bis(hydroxymethyl)furan (Figure 26d).<sup>[17]</sup> Kohtani et al. used photocharged commercial  $\text{TiO}_2(e^-/H^+)$  P25 to reduce substituted acetophenones to the corresponding alcohols (Figure 26e).<sup>[77,155]</sup> They confirmed that the ketones with less negative reduction potential can extract more electrons from  $\text{TiO}_2(e^-/H^+)$ . Graphitic carbon nitride materials enable  $2e^-/2H^+$  reduction of  $\text{O}_2$  to  $\text{H}_2\text{O}_2$ .<sup>[153,156]</sup> Li et al. applied  $\text{TiO}_2(e^-/H^+)$  for conversion of epoxides to alkenes (Figure 26f).<sup>[113]</sup> It was concluded that the reaction proceeds via concerted multielectron transfer.

### 9.3. $6e^-/6H^+$ Transfer

Reduction of nitroarenes to aromatic amines has been accomplished by  $\text{TiO}_2(e^-/H^+)$ ,<sup>[132]</sup> V-doped  $\text{V-TiO}_2(e^-/H^+)$ <sup>[66]</sup> and

$\text{K-PHI}(e^-/H^+)$ <sup>[36]</sup> (Figure 27). Unlike to reduction of nitrocompounds employing semiconductors under continuous illumination, which typically gives a range of products, such as diazo-, azoxy-, nitroso-compounds, and *N*-hydroxylamines,<sup>[157]</sup> photocharged  $\text{SCP}(e^-/H^+)$  yields selectively amines likely due to plenty of electrons and protons readily available for multi-electron transfer. Functional groups bearing multiple bonds, such as  $-\text{C}(\text{O})\text{Me}$ ,  $-\text{C}(\text{O})\text{OMe}$ ,  $-\text{C}\equiv\text{N}$ , and even C–halides bonds remained intact, likely due to intrinsically higher reactivity of  $\text{NO}_2$ -group toward electrons and protons stored in  $\text{SCP}(e^-/H^+)$ .<sup>[66]</sup>

Organic transformations summarized in Figures 25–27 can be performed using nano- and microsized materials composed of earth abundant elements in place of expensive noble metals, such as Ru and Ir. Combined with rechargeability of the semiconductors under illumination with UV–vis, the concept can pave way for a new direction in the field of organic synthesis.

## 10. Toward the Material Ideal for Photocharging

Analysis of data presented in Section 6 allows ranging the influence of materials properties as well as conditions under which photocharging is conducted on  $\delta_{\text{max}}$  in the following order: nature of SCP > structure of ED > type of counter ion > material  $S_{\text{SA}}$  >  $C_{\text{ED}}$ . Parameters on the left side of the scale have the highest impact on  $\delta_{\text{max}}$ , while those on the right have

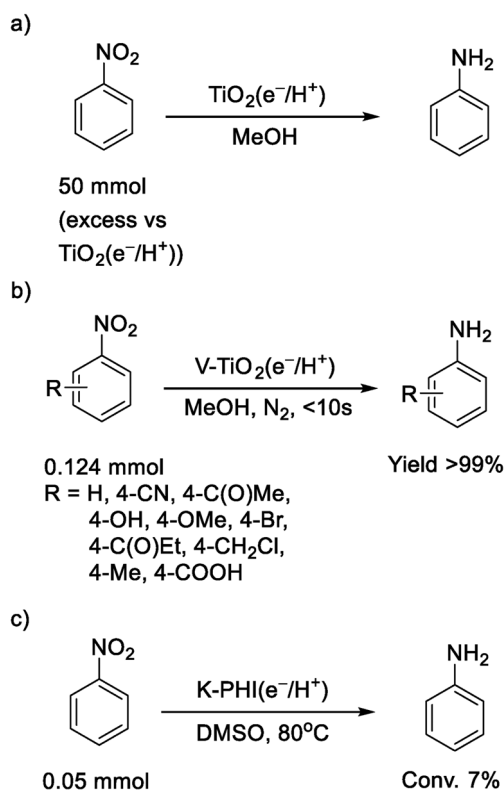


**Figure 27.** 6e<sup>-</sup>/6H<sup>+</sup> reduction of nitrocompounds to anilines mediated by SCP(e<sup>-</sup>/H<sup>+</sup>).

less significant influence. For example, higher  $\delta_{\max}$  values are reached by increasing  $C_{\text{ED}}$  and  $S_{\text{SA}}$ . At the same  $C_{\text{ED}}$  and  $S_{\text{SA}}$ , Ti-based SCPs possess higher  $\delta_{\max}$  compared to Zn-based SCPs. Sections 6 and 8 proved that  $R_{\text{PC}}$  and  $R_{\text{DC}}$  correlate with  $\delta_{\max}$ . Therefore, high capacity in a fully charged state is a key factor for materials to accumulate and release e<sup>-</sup>/X<sup>+</sup> fast.

What structural features of a material are the most important to attain the highest capacity in e<sup>-</sup>/H<sup>+</sup> storage and as a result fast rates of photocharging and discharging? Without doubts, community working in the area of materials photocharging can learn from the branch of materials science focused on electric charging of materials, batteries, and capacitors. In photocharging, however, the driving force is defined by the CB and VB potentials and supplied by incident light rather than electromotive force of a potentiostat. Therefore, unlike electric charging, photocharging proceeds under equilibrium conditions. From this standpoint, semiconductors with wider optical gap provide stronger driving force for the photoinduced electron transfer (see Equations (1) and (2)). It is beneficial to extract e<sup>-</sup>/H<sup>+</sup> not only from electron rich molecules, such as amines and alcohols, but also from electron deficient and ideally from one of the most abundant electron donors—water, VB potential in a semiconductor need to be highly positive (Figure 1). While TiO<sub>2</sub>-WO<sub>3</sub> hybrid composites are indeed photocharged at the expense of water vapor,<sup>[18,138]</sup> K-PHI with its VB potential of +2.2 V versus NHE, on the other hand, is capable to extract e<sup>-</sup>/H<sup>+</sup> from toluene.<sup>[152]</sup> Less negative CB potential of the semiconductor is also beneficial to suppress back electron transfer from SCP(e<sup>-</sup>/H<sup>+</sup>)—electrons in such specie occupy

thermodynamically more stable states. Semiconductors with optical gap <3.1 eV, such as ionic carbon nitrides,<sup>[43]</sup> are beneficial as they can accumulate e<sup>-</sup>/H<sup>+</sup> by harvesting larger portion of electromagnetic spectrum.

MOFs microporous structure and modulation of the chemical environment inside the micropore by adding guest molecules and ions improve conductivity of these materials via hopping transport.<sup>[158,159]</sup> Photocharging of microporous ionic carbon nitrides (Figure 3) discussed in this review outlines a rational approach for designing transition metal free materials with similar function. Covalent organic frameworks (COFs) carrying negative charge in their polymeric network are promising materials for photocharging. For example, COFs constructed from  $\gamma$ -cyclodextrine, negatively charged spiroborate linkers, and various counterions, such as Li<sup>+</sup>, dimethylammonium, piperazinium, possess high Li<sup>+</sup> conductivity of up to 2.7 mS cm<sup>-1</sup> at 30 °C.<sup>[160]</sup>

Excited state of certain organic cationic dyes, such as methylviologen,<sup>[161]</sup> Rhodamine 6G,<sup>[162]</sup> [Mes-Acr][BF<sub>4</sub>],<sup>[163]</sup> is quenched reductively by electron donors and as a result form persistent radicals. Such radicals are indefinitely stable under anaerobic conditions and may be considered as equivalents of photocharged SCP(e<sup>-</sup>/H<sup>+</sup>).  $\delta_{\max}$  values for the abovementioned radicals are 2.1–4.9 mmol[e<sup>-</sup>] g<sup>-1</sup>, defined by the molar mass of the dye and in general exceed  $\delta_{\max}$  of ZnO(e<sup>-</sup>/H<sup>+</sup>). Construction of microporous COFs that possess photoredox active moieties and interconnected by low-molecular weight linkers might provide a class of materials with high  $\delta_{\max}$ .<sup>[164–166]</sup> Overall, microporous structure, high ionic conductivity, and highly positive VB potential are three the most important parameters to reach high  $\delta_{\max}$ ,  $R_{\text{PC}}$ , and  $R_{\text{DC}}$ .

## 11. Conclusions and Outlook

Fifty two research articles that deal with photocharging of materials were analyzed, from which a data set of several hundreds entries was compiled. Based on database analysis the following conclusions could be made.

- 1) Higher  $\delta_{\max}$  values are typically obtained for semiconductors that are made of elements capable to adopt stable lower oxidation states such as +3 in TiO<sub>2</sub>. Stronger reductants afford higher  $\delta_{\max}$ . Using organometallic reagents, many of which are strong reductants, affords higher  $\delta_{\max}$  along with intercalation of M<sup>n+</sup> counter ions instead of H<sup>+</sup>.
- 2)  $\langle n_{\max} \rangle$  scales with the volume of semiconductor particle, which is explained by the fact that electrons and small charge-compensating cations are distributed in the bulk of semiconductors.
- 3) When conditions of photocharging are kept the same, for 0.95–21 nm particles,  $R_{\text{PC}}$  scales linearly with  $\delta_{\max}$ , which may be explained by fast intercalation of small counter ions into the bulk of the material or adsorption of large cations on the surface.
- 4) For nonporous semiconductor particles,  $R_{\text{DC}}$  decreases with particle volume, while microporous structure of Ti-based MOFs that facilitates ion transport allows retaining relatively high  $R_{\text{DC}}$  even for micrometer-sized particles.
- 5) For 4.1–21 nm nonporous ZnO and TiO<sub>2</sub> as well as >100 nm microporous poly(heptazine imide) particles,  $R_{\text{DC}}$

scales linearly with initial concentration of electrons in photocharged materials. It may be explained by stronger driving force for electron transfer from the photocharged semiconductor to the oxidant exerted by the Fermi level shift. Alternatively, it may be explained by the fact that discharging of the semiconductor is a bimolecular process with the velocity proportional to the product of oxidant concentration and concentration of electrons in the photocharged semiconductor.

- 6) Stronger oxidants remove electrons from the photocharged semiconductor faster.

Already now, a database of photocharged materials may be used by data scientists in combination with machine learning to derive hidden dependencies between  $\langle n \rangle$ ,  $\delta$ ,  $R_{PC}$ ,  $R_{DC}$ , and materials structure as well as parameters of materials photocharging and discharging in dark. Taking into account increasing number of publications in this area of research, the database will be extended in future.

Due to plenty of electrons available in photocharged semiconductors at nearly the same potential, at least one example—reductive dimerization of enones—unambiguously point that reactivity of semiconductor particles under continuous light illumination (classical photocatalysis)<sup>[151]</sup> and semiconductors photocharged with  $e^-/H^+$  (ref. [36]) is different. Studying photocharged SCP( $e^-/H^+$ ) as PCET reagents may establish a whole new field of preparative organic chemistry.

This review focuses exclusively on n-type semiconductors charged with electrons and charge-compensating cations. Semiconductors loaded with holes and charge-compensating anions SCP( $h^+/Y^-$ ) is even less explored class of materials.<sup>[167]</sup> SCP( $h^+/Y^-$ ) carrying either simple halides,  $Y^- = F^-, Cl^-, Br^-$ , or more complex anions may also be used for functionalization of organic compounds and extend the borders of preparative organic chemistry.

## Acknowledgements

O.S. thanks Roy Pftzner and Jan Scharein for their help in setting up pemat.mpg.de, Max Plank Society for providing subscription to journals and Prof. Markus Antonietti for fruitful discussion.

Open access funding enabled and organized by Projekt DEAL.

## Conflict of Interest

The author declares no conflict of interest.

## Keywords

hydrogen storage, organic synthesis, photocatalysis, photocharging, photodoping, semiconductors, solar batteries

Received: January 28, 2022

Revised: March 21, 2022

Published online: April 16, 2022

[1] G.-M. Schwab, H. Noller, F. Steinbach, M. Venugopalan, *Nature* **1962**, 193, 774.

[2] H. Nishiyama, T. Yamada, M. Nakabayashi, Y. Maehara, M. Yamaguchi, Y. Kuromiya, Y. Nagatsuma, H. Tokudome,

- S. Akiyama, T. Watanabe, R. Narushima, S. Okunaka, N. Shibata, T. Takata, T. Hisatomi, K. Domen, *Nature* **2021**, 598, 304.
- [3] A. Savateev, I. Ghosh, B. König, M. Antonietti, *Angew. Chem., Int. Ed.* **2018**, 57, 15936.
- [4] B. Ohtani, B. Pal, S. Ikeda, *Catal. Surv. Asia* **2003**, 7, 165.
- [5] H. Kisch, *Angew. Chem., Int. Ed.* **2013**, 52, 812.
- [6] N. A. Romero, D. A. Nicewicz, *Chem. Rev.* **2016**, 116, 10075.
- [7] D. Rehm, A. Weller, *Ber. Bunsen-Ges. Phys. Chem.* **1969**, 73, 834.
- [8] A. Fujishima, X. Zhang, D. A. Tryk, *Surf. Sci. Rep.* **2008**, 63, 515.
- [9] X. Wang, C. Li, *J. Photochem. Photobiol., C* **2017**, 33, 165.
- [10] R. A. Marcus, *Angew. Chem., Int. Ed. Engl.* **1993**, 32, 1111.
- [11] C. Harris, P. V. Kamat, *ACS Nano* **2009**, 3, 682.
- [12] I. Bedja, S. Hotchandani, P. V. Kamat, *J. Phys. Chem.* **1993**, 97, 11064.
- [13] H. Kasap, C. A. Caputo, B. C. M. Martindale, R. Godin, V. W.-h. Lau, B. V. Lotsch, J. R. Durrant, E. Reisner, *J. Am. Chem. Soc.* **2016**, 138, 9183.
- [14] G. M. Carroll, A. M. Schimpf, E. Y. Tsui, D. R. Gamelin, *J. Am. Chem. Soc.* **2015**, 137, 11163.
- [15] A. Henglein, *Ber. Bunsen-Ges. Phys. Chem.* **1982**, 86, 241.
- [16] R. F. Howe, M. Gratzel, *J. Phys. Chem.* **1985**, 89, 4495.
- [17] S. Qiao, Y. Zhou, H. Hao, X. Liu, L. Zhang, W. Wang, *Green Chem.* **2019**, 21, 6585.
- [18] S. Higashimoto, T. Shishido, Y. Ohno, M. Azuma, M. Takahashi, M. Anpo, *J. Electrochem. Soc.* **2007**, 154, F48.
- [19] W. Zhao, X.-F. Wang, E. Zheng, Y. Wei, Y. Sanehira, G. Chen, *J. Power Sources* **2017**, 350, 28.
- [20] C. N. Valdez, A. M. Schimpf, D. R. Gamelin, J. M. Mayer, *J. Am. Chem. Soc.* **2016**, 138, 1377.
- [21] J. Schneider, M. Matsuoka, M. Takeuchi, J. Zhang, Y. Horiuchi, M. Anpo, D. W. Bahnemann, *Chem. Rev.* **2014**, 114, 9919.
- [22] H. H. Mohamed, D. W. Bahnemann, *Appl. Catal., B* **2012**, 128, 91.
- [23] L. Zhang, H. H. Mohamed, R. Dillert, D. Bahnemann, *J. Photochem. Photobiol., C* **2012**, 13, 263.
- [24] B. Sulzberger, H. Laubscher, *Mar. Chem.* **1995**, 50, 103.
- [25] F. F. Marafatto, M. L. Strader, J. Gonzalez-Holguera, A. Schwartzberg, B. Gilbert, J. Peña, *Proc. Natl. Acad. Sci. USA* **2015**, 112, 4600.
- [26] V. Seminko, P. Maksimchuk, O. Avrunin, V. Semenets, Y. Malyukin, *Phys. Status Solidi B* **2019**, 256, 1900325.
- [27] D. Damatov, S. M. Laga, E. A. Mader, J. Peng, R. G. Agarwal, J. M. Mayer, *Inorg. Chem.* **2018**, 57, 14401.
- [28] H. Miyazaki, N. Eimori, T. Matsuura, T. Ota, *J. Mater. Sci. Res.* **2018**, 7, 9.
- [29] X. Dong, Y. Wei, J. Gao, X. Liu, L. Zhang, Y. Tong, Y. Lu, *J. Photochem. Photobiol., A* **2022**, 425, 113716.
- [30] G. Poirier, M. Nalin, Y. Messaddeq, S. J. L. Ribeiro, *Solid State Ionics* **2007**, 178, 871.
- [31] P. Gómez-Romero, *Solid State Ionics* **1997**, 101–103, 243.
- [32] T. Yamase, *Chem. Rev.* **1998**, 98, 307.
- [33] P. Gómez-Romero, N. Casañ-Pastor, *J. Phys. Chem.* **1996**, 100, 12448.
- [34] V. W.-H. Lau, D. Klose, H. Kasap, F. Podjaski, M.-C. Pignié, E. Reisner, G. Jeschke, B. V. Lotsch, *Angew. Chem., Int. Ed.* **2017**, 56, 510.
- [35] Y. Markushyna, P. Lamagni, C. Teutloff, J. Catalano, N. Lock, G. Zhang, M. Antonietti, A. Savateev, *J. Mater. Chem. A* **2019**, 7, 24771.
- [36] S. Mazzanti, C. Schritt, K. ten Brummelhuis, M. Antonietti, A. Savateev, *Exploration* **2021**, 1, 20210063.
- [37] F. Podjaski, J. Kröger, B. V. Lotsch, *Adv. Mater.* **2018**, 30, 1705477.
- [38] H. Schlömerberg, J. Kröger, G. Savasci, M. W. Terban, S. Bette, I. Moudrakovski, V. Duppel, F. Podjaski, R. Siegel, J. Senker, R. E. Dinnebier, C. Ochsenfeld, B. V. Lotsch, *Chem. Mater.* **2019**, 31, 7478.
- [39] A. Savateev, N. V. Tarakina, V. Strauss, T. Hussain, K. ten Brummelhuis, J. M. Sánchez Vadillo, Y. Markushyna, S. Mazzanti, A. P. Tyutyunnik, R. Walczak, M. Oschatz, D. M. Guldi, A. Karton, M. Antonietti, *Angew. Chem., Int. Ed.* **2020**, 59, 15061.
- [40] S. K. Sahoo, I. F. Teixeira, A. Naik, J. Heske, D. Cruz, M. Antonietti, A. Savateev, T. D. Kühne, *J. Phys. Chem. C* **2021**, 125, 13749.

- [41] M. A. R. da Silva, I. F. Silva, Q. Xue, B. T. W. Lo, N. V. Tarakina, B. N. Nunes, P. Adler, S. K. Sahoo, D. W. Bahnemann, N. López-Salas, A. Savateev, C. Ribeiro, T. D. Kühne, M. Antonietti, I. F. Teixeira, *Appl. Catal., B* **2022**, *304*, 120965.
- [42] B. V. Lotsch, M. Döblinger, J. Sehnert, L. Seyfarth, J. Senker, O. Oeckler, W. Schnick, *Chem. – Eur. J.* **2007**, *13*, 4969.
- [43] A. Savateev, M. Antonietti, *ChemCatChem* **2019**, *11*, 6166.
- [44] J. Kröger, F. Podjaski, G. Savasci, I. Moudrakovski, A. Jiménez-Solano, M. W. Terban, S. Bette, V. Duppel, M. Joos, A. Senocrate, R. Dinnebieer, C. Ochsenfeld, B. V. Lotsch, *Adv. Mater.* **2022**, *34*, 2107061.
- [45] C. T. Saouma, S. Richard, S. Smolders, M. F. Delley, R. Ameloot, F. Vermoortele, D. E. De Vos, J. M. Mayer, *J. Am. Chem. Soc.* **2018**, *140*, 16184.
- [46] M. Dan-Hardi, C. Serre, T. Frot, L. Rozes, G. Maurin, C. Sanchez, G. Férey, *J. Am. Chem. Soc.* **2009**, *131*, 10857.
- [47] Y. Fu, D. Sun, Y. Chen, R. Huang, Z. Ding, X. Fu, Z. Li, *Angew. Chem., Int. Ed.* **2012**, *51*, 3364.
- [48] B. Bueken, F. Vermoortele, D. E. P. Vanpoucke, H. Reinsch, C.-C. Tsou, P. Valvekens, T. De Baerdemaeker, R. Ameloot, C. E. A. Kirschhock, V. Van Speybroeck, J. M. Mayer, D. De Vos, *Angew. Chem., Int. Ed.* **2015**, *54*, 13912.
- [49] M. J. Turo, L. Chen, C. E. Moore, A. M. Schimpf, *J. Am. Chem. Soc.* **2019**, *141*, 4553.
- [50] A. I. Kuznetsov, O. Kameneva, N. Bityurin, L. Rozes, C. Sanchez, A. Kanaev, *Phys. Chem. Chem. Phys.* **2009**, *11*, 1248.
- [51] M. Jakob, H. Levanon, P. V. Kamat, *Nano Lett.* **2003**, *3*, 353.
- [52] F. N. Castellano, J. M. Stipkala, L. A. Friedman, G. J. Meyer, *Chem. Mater.* **1994**, *6*, 2123.
- [53] A. Agrawal, S. H. Cho, O. Zandi, S. Ghosh, R. W. Johns, D. J. Milliron, *Chem. Rev.* **2018**, *118*, 3121.
- [54] I. Kriegel, F. Scotognella, L. Manna, *Phys. Rep.* **2017**, *674*, 1.
- [55] Y. Ke, J. Chen, G. Lin, S. Wang, Y. Zhou, J. Yin, P. S. Lee, Y. Long, *Adv. Energy Mater.* **2019**, *9*, 1902066.
- [56] M. Ghini, N. Curreli, A. Camellini, M. Wang, A. Asaithambi, I. Kriegel, *Nanoscale* **2021**, *13*, 8773.
- [57] V. Sridhar, F. Podjaski, J. Kröger, A. Jiménez-Solano, B.-W. Park, B. V. Lotsch, M. Sitti, *Proc. Natl. Acad. Sci. USA* **2020**, *117*, 24748.
- [58] V. Sridhar, F. Podjaski, Y. Alapan, J. Kröger, L. Grunenberg, V. Kishore, B. V. Lotsch, M. Sitti, *Sci. Rob.* **2022**, *7*, 1421.
- [59] C. Chen, T. Shi, W. Chang, J. Zhao, *ChemCatChem* **2015**, *7*, 724.
- [60] S. Kohtani, A. Kawashima, H. Miyabe, *Catalysts* **2017**, *7*, 303.
- [61] M. Mokhtarifar, D. T. Nguyen, M. V. Diamanti, R. Kaveh, M. Asa, M. Sakar, M. Pedferri, T.-O. Do, *New J. Chem.* **2020**, *44*, 20375.
- [62] F. Feng, W. Yang, S. Gao, C. Sun, Q. Li, *ACS Sustainable Chem. Eng.* **2018**, *6*, 6166.
- [63] T. Cai, Y. Liu, L. Wang, W. Dong, G. Zeng, *J. Photochem. Photobiol., C* **2019**, *39*, 58.
- [64] A. M. Schimpf, C. E. Gunthardt, J. D. Rinehart, J. M. Mayer, D. R. Gamelin, *J. Am. Chem. Soc.* **2013**, *135*, 16569.
- [65] J. N. Schrauben, R. Hayoun, C. N. Valdez, M. Braten, L. Fridley, J. M. Mayer, *Science* **2012**, *336*, 1298.
- [66] J. Su, X.-X. Zou, G.-D. Li, L. Li, J. Zhao, J.-S. Chen, *Chem. Commun.* **2012**, *48*, 9032.
- [67] S. Ikeda, N. Sugiyama, S.-y. Murakami, H. Kominami, Y. Kera, H. Noguchi, K. Uosaki, T. Torimoto, B. Ohtani, *Phys. Chem. Chem. Phys.* **2003**, *5*, 778.
- [68] J. Hu, L. Zhan, G. Zhang, Q. Zhang, L. Du, C.-H. Tung, Y. Wang, *Inorg. Chem.* **2016**, *55*, 8493.
- [69] P. Guyot-Sionnest, *Microchim. Acta* **2008**, *160*, 309.
- [70] M. Shim, P. Guyot-Sionnest, *Nature* **2000**, *407*, 981.
- [71] J. Kim, D. Choi, K. S. Jeong, *Chem. Commun.* **2018**, *54*, 8435.
- [72] M. Zikmund, L. Štepičková, M. Kohútová, *Chem. Zvesti* **1969**, *23*, 856.
- [73] T. Krämer, F. Tuna, S. D. Pike, *Chem. Sci.* **2019**, *10*, 6886.
- [74] The  $\varepsilon$  value was estimated from the absorption spectrum of photo-charged  $\text{Ti}_4$ . The  $\varepsilon$  value depends on the degree of  $\text{Ti}_4$ -oxo-alkoxide clusters photoreduction and as a result on the illumination time.
- [75] A. I. Kuznetsov, O. Kameneva, A. Alexandrov, N. Bityurin, P. Marreau, K. Chhor, C. Sanchez, A. Kanaev, *Phys. Rev. E* **2005**, *71*, 021403.
- [76] C. Kormann, D. W. Bahnemann, M. R. Hoffmann, *J. Phys. Chem.* **1988**, *92*, 5196.
- [77] S. Kohtani, E. Yoshioka, K. Saito, A. Kudo, H. Miyabe, *J. Phys. Chem. C* **2012**, *116*, 17705.
- [78] H. H. Mohamed, C. B. Mendive, R. Dillert, D. W. Bahnemann, *J. Phys. Chem. A* **2011**, *115*, 2139.
- [79] U. Koelle, J. Moser, M. Graetzel, *Inorg. Chem.* **1985**, *24*, 2253.
- [80] A. Safrany, R. Gao, J. Rabani, *J. Phys. Chem. B* **2000**, *104*, 5848.
- [81] A. Kongkanand, P. V. Kamat, *ACS Nano* **2007**, *1*, 13.
- [82] H. Hartmann, H. L. Schläfer, K. H. Hansen, *Z. Anorg. Allg. Chem.* **1956**, *284*, 153.
- [83] R. Hayoun, K. M. Whitaker, D. R. Gamelin, J. M. Mayer, *J. Am. Chem. Soc.* **2011**, *133*, 4228.
- [84] K. M. Whitaker, S. T. Ochsenbein, V. Z. Polinger, D. R. Gamelin, *J. Phys. Chem. C* **2008**, *112*, 14331.
- [85] E. Y. Martinez, K. Zhu, C. W. Li, *Nano Lett.* **2020**, *20*, 7580.
- [86] U. Joost, A. Šutka, M. Oja, K. Smits, N. Döbelin, A. Loot, M. Järvekülg, M. Hirsimäki, M. Valden, E. Nömmiste, *Chem. Mater.* **2018**, *30*, 8968.
- [87] C. N. Valdez, M. F. Delley, J. M. Mayer, *J. Am. Chem. Soc.* **2018**, *140*, 8924.
- [88] R. Asahi, Y. Taga, W. Mannstadt, A. J. Freeman, *Phys. Rev. B* **2000**, *61*, 7459.
- [89] M. Takeuchi, G. Martra, S. Coluccia, M. Anpo, *J. Phys. Chem. C* **2007**, *111*, 9811.
- [90] E. Y. Tsui, K. H. Hartstein, D. R. Gamelin, *J. Am. Chem. Soc.* **2016**, *138*, 11105.
- [91] Y. Lin, Y. Yan, W. Peng, X. Qiao, D. Huang, H. Ji, C. Chen, W. Ma, J. Zhao, *J. Phys. Chem. Lett.* **2020**, *11*, 3941.
- [92] I. Resa, E. Carmona, E. Gutierrez-Puebla, A. Monge, *Science* **2004**, *305*, 1136.
- [93] A. M. Schimpf, K. E. Knowles, G. M. Carroll, D. R. Gamelin, *Acc. Chem. Res.* **2015**, *48*, 1929.
- [94] C. Y. Liu, A. J. Bard, *J. Phys. Chem.* **1989**, *93*, 3232.
- [95] J. Castillo-Lora, R. Mitsunashi, J. M. Mayer, *J. Phys. Chem. C* **2019**, *123*, 10262.
- [96] J. Castillo-Lora, M. F. Delley, S. M. Laga, J. M. Mayer, *J. Phys. Chem. Lett.* **2020**, *11*, 7687.
- [97] L. Capaldo, D. Ravelli, *Eur. J. Org. Chem.* **2017**, *2017*, 2056.
- [98] L. Capaldo, D. Ravelli, M. Fagnoni, *Chem. Rev.* **2021**.
- [99] N. Berg, S. Bergwinkl, P. Nuernberger, D. Horinek, R. M. Gschwind, *J. Am. Chem. Soc.* **2021**, *143*, 724.
- [100] Z. Hou, T. Miyano, H. Yamazaki, Y. Wakatsuki, *J. Am. Chem. Soc.* **1995**, *117*, 4421.
- [101] O. P. Lam, C. Anthon, F. W. Heinemann, J. M. O'Connor, K. Meyer, *J. Am. Chem. Soc.* **2008**, *130*, 6567.
- [102] S. Shi, R. Szostak, M. Szostak, *Org. Biomol. Chem.* **2016**, *14*, 9151.
- [103] J. J. Warren, T. A. Tronic, J. M. Mayer, *Chem. Rev.* **2010**, *110*, 6961.
- [104] S. R. Morrison, T. Freund, *J. Chem. Phys.* **1967**, *47*, 1543.
- [105] Z. Wang, M. G. Mathews, B. Koplitz, *J. Phys. Chem.* **1995**, *99*, 6913.
- [106] E. Baciocchi, M. Bietti, O. Lanzalunga, *Acc. Chem. Res.* **2000**, *33*, 243.
- [107] Y. Markushyna, P. Lamagni, J. Catalano, N. Lock, G. Zhang, M. Antonietti, A. Savateev, *ACS Catal.* **2020**, *10*, 7336.
- [108] D. Franchi, Z. Amara, *ACS Sustainable Chem. Eng.* **2020**, *8*, 15405.
- [109] Y. Yan, W. Shi, W. Peng, Y. Lin, C. Zhang, L. Li, Y. Sun, H. Ju, J. Zhu, W. Ma, J. Zhao, *Commun. Chem.* **2019**, *2*, 88.
- [110] F. Su, S. C. Mathew, L. Möhlmann, M. Antonietti, X. Wang, S. Blechert, *Angew. Chem., Int. Ed.* **2011**, *50*, 657.
- [111] M. A. Bajada, A. Vijeta, A. Savateev, G. Zhang, D. Howe, E. Reisner, *ACS Appl. Mater. Interfaces* **2020**, *12*, 8176.
- [112] A. M. Schimpf, S. D. Lounis, E. L. Runnerstrom, D. J. Milliron, D. R. Gamelin, *J. Am. Chem. Soc.* **2015**, *137*, 518.



- [113] Y. Li, H. Ji, C. Chen, W. Ma, J. Zhao, *Angew. Chem., Int. Ed.* **2013**, 52, 12636.
- [114] D. Zhao, C. Chen, C. Yu, W. Ma, J. Zhao, *J. Phys. Chem. C* **2009**, 113, 13160.
- [115] T. Watanabe, K. Honda, *J. Phys. Chem.* **1982**, 86, 2617.
- [116] Y. D. Iorio, M. E. Aguirre, M. A. Brusa, M. A. Grela, *J. Phys. Chem. C* **2012**, 116, 9646.
- [117] S. Zeng, L. Zhang, W. Wang, D. Shao, H. Hao, *Phys. Chem. Chem. Phys.* **2017**, 19, 29053.
- [118] A. M. Schimpf, S. T. Ochsenbein, R. Buonsanti, D. J. Milliron, D. R. Gamelin, *Chem. Commun.* **2012**, 48, 9352.
- [119] J. A. Fauchaux, P. K. Jain, *J. Phys. Chem. Lett.* **2013**, 4, 3024.
- [120] C. Wang, M. Shim, P. Guyot-Sionnest, *Science* **2001**, 291, 2390.
- [121] P. Hoyer, H. Weller, *Chem. Phys. Lett.* **1994**, 221, 379.
- [122] H. H. Mohamed, N. A. Alomair, D. W. Bahnemann, *Arabian J. Chem.* **2019**, 12, 5134.
- [123] W. K. Liu, K. M. Whitaker, A. L. Smith, K. R. Kittilstved, B. H. Robinson, D. R. Gamelin, *Phys. Rev. Lett.* **2007**, 98, 186804.
- [124] C. N. Valdez, M. Braten, A. Soria, D. R. Gamelin, J. M. Mayer, *J. Am. Chem. Soc.* **2013**, 135, 8492.
- [125] G. Rothenberger, D. Fitzmaurice, M. Graetzel, *J. Phys. Chem.* **1992**, 96, 5983.
- [126] J. Wang, J. Polleux, J. Lim, B. Dunn, *J. Phys. Chem. C* **2007**, 111, 14925.
- [127] H. Lindström, S. Södergren, A. Solbrand, H. Rensmo, J. Hjelm, A. Hagfeldt, S.-E. Lindquist, *J. Phys. Chem. B* **1997**, 101, 7717.
- [128] <https://public.tableau.com/app/profile/oleksandr.savatieiev> (accessed: January 2022).
- [129] M. N. Braten, D. R. Gamelin, J. M. Mayer, *ACS Nano* **2015**, 9, 10258.
- [130] K. Ip, M. E. Overberg, Y. W. Heo, D. P. Norton, S. J. Pearton, C. E. Stutz, B. Luo, F. Ren, D. C. Look, J. M. Zavada, *Appl. Phys. Lett.* **2003**, 82, 385.
- [131] R. Hengerer, L. Kavan, P. Krtil, M. Grätzel, *J. Electrochem. Soc.* **2000**, 147, 1467.
- [132] X.-X. Zou, G.-D. Li, K.-X. Wang, L. Li, J. Su, J.-S. Chen, *Chem. Commun.* **2010**, 46, 2112.
- [133] Z. Chen, A. Savateev, S. Pronkin, V. Papaefthimiou, C. Wolff, M. G. Willinger, E. Willinger, D. Neher, M. Antonietti, D. Dontsova, *Adv. Mater.* **2017**, 29, 1700555.
- [134] I. F. Teixeira, N. V. Tarakina, I. F. Silva, N. López-Salas, A. Savateev, M. Antonietti, *Adv. Sustainable Syst.* **2022**, 2100429.
- [135] C. Adler, S. Selim, I. Kivrtsov, C. Li, D. Mitoraj, B. Dietzek, J. R. Durrant, R. Beranek, *Adv. Funct. Mater.* **2021**, 31, 2105369.
- [136] R. Costi, A. E. Saunders, E. Elmalem, A. Salant, U. Banin, *Nano Lett.* **2008**, 8, 637.
- [137] P. D. Cozzoli, M. L. Curri, A. Agostiano, *Chem. Commun.* **2005**, 3186.
- [138] P. Ngaotakanwivat, T. Tatsuma, *J. Electroanal. Chem.* **2004**, 573, 263.
- [139] C. Li, E. Hofmeister, I. Kivrtsov, D. Mitoraj, C. Adler, R. Beranek, B. Dietzek, *ChemSusChem* **2021**, 14, 1728.
- [140] P. Ngaotakanwivat, T. Tatsuma, S. Saitoh, Y. Ohko, A. Fujishima, *Phys. Chem. Chem. Phys.* **2003**, 5, 3234.
- [141] A. Wood, M. Giersig, P. Mulvaney, *J. Phys. Chem. B* **2001**, 105, 8810.
- [142] Data is not shown in Figure 18 since the source does not explicitly specify if saturation of a material with electrons was reached.
- [143] A. Kongkanand, P. V. Kamat, *J. Phys. Chem. C* **2007**, 111, 9012.
- [144] S. O. Obare, T. Ito, G. J. Meyer, *J. Am. Chem. Soc.* **2006**, 128, 712.
- [145] H. H. Mohamed, R. Dillert, D. W. Bahnemann, *J. Phys. Chem. C* **2011**, 115, 12163.
- [146] V. Subramanian, E. E. Wolf, P. V. Kamat, *J. Am. Chem. Soc.* **2004**, 126, 4943.
- [147] D. W. Bahnemann, M. Hilgendorff, R. Memming, *J. Phys. Chem. B* **1997**, 101, 4265.
- [148] V. V. Pavlishchuk, A. W. Addison, *Inorg. Chim. Acta* **2000**, 298, 97.
- [149] R. J. Enemærke, T. B. Christensen, H. Jensen, K. Daasbjerg, *J. Chem. Soc., Perkin Trans. 2* **2001**, 1620.
- [150] J. M. Meichtry, R. Dillert, D. W. Bahnemann, M. I. Litter, *Langmuir* **2015**, 31, 6229.
- [151] B. Kurpil, Y. Markushyna, A. Savateev, *ACS Catal.* **2019**, 9, 1531.
- [152] A. Savateev, B. Kurpil, A. Mishchenko, G. Zhang, M. Antonietti, *Chem. Sci.* **2018**, 9, 3584.
- [153] Z. Zeng, X. Quan, H. Yu, S. Chen, Y. Zhang, H. Zhao, S. Zhang, *Appl. Catal., B* **2018**, 236, 99.
- [154] B. Kurpil, K. Otte, A. Mishchenko, P. Lamagni, W. Lipiński, N. Lock, M. Antonietti, A. Savateev, *Nat. Commun.* **2019**, 10, 945.
- [155] S. Kohtani, Y. Kamoi, E. Yoshioka, H. Miyabe, *Catal. Sci. Technol.* **2014**, 4, 1084.
- [156] H. Ou, C. Tang, X. Chen, M. Zhou, X. Wang, *ACS Catal.* **2019**, 9, 2949.
- [157] L. Pei, H. Tan, M. Liu, R. Wang, X. Gu, X. Ke, J. Jia, Z. Zheng, *Green Chem.* **2021**, 23, 3612.
- [158] L. Sun, M. G. Campbell, M. Dincă, *Angew. Chem., Int. Ed.* **2016**, 55, 3566.
- [159] M. Sadakiyo, T. Yamada, H. Kitagawa, *J. Am. Chem. Soc.* **2014**, 136, 13166.
- [160] Y. Zhang, J. Duan, D. Ma, P. Li, S. Li, H. Li, J. Zhou, X. Ma, X. Feng, B. Wang, *Angew. Chem., Int. Ed.* **2017**, 56, 16313.
- [161] B. Xiang, L. Kevan, *J. Phys. Chem.* **1994**, 98, 5120.
- [162] I. Ghosh, B. König, *Angew. Chem., Int. Ed.* **2016**, 55, 7676.
- [163] I. A. MacKenzie, L. Wang, N. P. R. Onuska, O. F. Williams, K. Begam, A. M. Moran, B. D. Dunietz, D. A. Nicewicz, *Nature* **2020**, 580, 76.
- [164] Z. Mi, T. Zhou, W. Weng, J. Unruangsri, K. Hu, W. Yang, C. Wang, K. A. I. Zhang, J. Guo, *Angew. Chem., Int. Ed.* **2021**, 60, 9642.
- [165] G. Das, S. K. Sharma, T. Prakasam, F. Gándara, R. Mathew, N. Alkhatib, N. i. Saleh, R. Pasricha, J.-C. Olsen, M. Baias, S. Kirmizialtin, R. Jagannathan, A. Trabolsi, *Commun. Chem.* **2019**, 2, 106.
- [166] C. Zhang, J. Guo, X. Zou, S. Guo, Y. Guo, R. Shi, F. Yan, *Adv. Healthcare Mater.* **2021**, 10, 2100775.
- [167] B. H. Meekins, P. V. Kamat, *J. Phys. Chem. Lett.* **2011**, 2, 2304.



**Oleksandr Savateev** received his Ph.D. degree in organic chemistry from the Institute of Organic Chemistry of the National Academy of Science of Ukraine in 2016. Shortly after defense of his thesis, he joined Colloid Chemistry department of the Max Planck Institute of Colloids and Interfaces, where he founded and continues leading his group “Innovative Heterogeneous Photocatalysis.” His research interests evolved from chemistry in solution to photochemistry at surfaces and voids of extended structures. He is convinced that discoveries are possible by applying old knowledge to current challenges.